Astrocyte Progenitors Derived From Patients With Alzheimer Disease Do Not Impair Stroke Recovery in Mice

Välimäki, Nelli-Noora

2022-10

Välimäki , N-N , Bakreen , A , Häkli , S , Dhungana , H , Keuters , M H , Dunlop , Y , Koskuvi , M , Keksa-Goldsteine , V , Oksanen , M , Jäntti , H , Lehtonen , S , Malm , T , Koistinaho , J & Jolkkonen , J 2022 , ' Astrocyte Progenitors Derived From Patients With Alzheimer Disease Do Not Impair Stroke Recovery in Mice ' , Stroke , vol. 53 , no. 10 , pp. 3192-3201 . https://doi.org/10.1161/S

http://hdl.handle.net/10138/356257
https://doi.org/10.1161/STROKEAHA.122.039700

unspecified
acceptedVersion

Astrocyte Progenitors Derived from Patients with Alzheimer's Disease Do Not Impair Stroke Recovery in Mice

Nelli-Noora Välimäki[1], MSc, Abdulhameed Bakreen[1], MSc, Sara Häkli[1], MSc, Hiramani Dhungana[1,2], PhD, Meike H. Keuters[1,2], PhD, Yannick Dunlop[1], BSc, Marja Koskuvi[1,2], PhD, Velta Keksa-Goldsteine[1], MSc, Minna Oksanen[1], MSc, Henna Jäntti[1], PhD, Šárka Lehtonen[1,2], PhD, Tarja Malm[1], PhD, Jari Koistinaho[1,2], MD, Jukka Jolkkonen[1], PhD

[1]A.I. Virtanen Institute for Molecular Sciences, University of Eastern Finland, Kuopio, Finland

[2]Neuroscience Center, HiLIFE Helsinki Institute of Life Science, University of Helsinki, Helsinki, Finland

Correspondence to Jukka Jolkkonen, A.I. Virtanen Institute for Molecular Sciences, University of Eastern Finland, Kuopio, Finland. Email: jukka.jolkkonen@uef.fi

BACKGROUND AND PURPOSE: Species-specific differences in astrocytes and their Alzheimer's disease (AD)-associated pathology may influence cellular responses to other insults. Herein, human glial chimeric mice were generated to evaluate how AD predisposing genetic background in human astrocytes contributes to behavioral outcome and brain pathology after cortical photothrombotic ischemia.

METHODS: Neonatal (P0) immunodeficient mice of both sexes were transplanted with induced pluripotent stem cell-derived astrocyte progenitors from AD patients carrying *PSEN1* exon 9 deletion (PSENdE9), with isogenic controls, with cells from a healthy donor, or with mouse astrocytes or phosphate buffered saline. After 14 months, a photothrombotic lesion was produced with Rose Bengal in the motor cortex. Behavior was assessed prior to ischemia and one and four weeks after the induction of stroke, followed by tissue perfusion for histology.

RESULTS: Open field, cylinder, and grid-walking tests showed a persistent locomotor and sensorimotor impairment after ischemia and female mice had larger infarct sizes, yet these were not affected by astrocytes with PSEN1dE9 background. Staining for human nuclear antigen confirmed that human cells successfully engrafted throughout the mouse brain. However, only a small number of human cells were positive for astrocytic marker glial fibrillary acidic protein (GFAP), mostly located in the corpus callosum and retaining complex human-specific morphology with longer processes compared to host counterparts. Whilst host astrocytes formed the glial scar, human astrocytes were scattered in small numbers close to the lesion boundary. Aβ deposits were not present in PSEN1 ΔE9 astrocyte-transplanted mice.

CONCLUSIONS: Transplanted human cells survived and distributed widely in the host brain but had no impact on severity of ischemic damage after cortical photothrombosis in chimeric mice. Only a small number of transplanted human astrocytes acquired GFAP-positive glial phenotype or migrated towards the ischemic lesion forming glial scar. PSEN1 ΔE9 astrocytes did not impair behavioral recovery after experimental stroke.

Graphic Abstract

Key Words: Alzheimer's disease ■ behavioral outcome ■ cortical stroke ■ glial chimeric mice ■ histology

Nonstandard Abbreviations and Acronyms

Aβ	Beta-amyloid
AD	Alzheimer's disease
AQP4	Aquaporin 4
CTRL	Control
DAPI	4′,6-Diamidino-2-phenylindole
DCX	Doublecortin
GFAP	Glial fibrillary acidic protein
hAD	Human iPSC-astrocyte progenitors derived from AD patients
hCTRL	Healthy donor control group
HuNu	Human nuclei
iCTRL	Isogenic control group
iPSC	Induced pluripotent stem cells
mCTRL	Mouse control group
PBS	Phosphate-buffered saline
PDGFRα	Platelet-derived growth factor receptor alpha
PSEN1	Presenilin 1
SVZ	Subventricular zone

Astrocytes play a central role in normal brain function by regulating blood flow, synaptic function and plasticity, as well as maintaining balance of extracellular ions, fluids, and transmitters.[1] In response to cerebral insults such as stroke, astrocytes undergo a complex process called reactive astrogliosis characterized by hypertrophy, proliferation, and scar formation.[2,3] Given that the changes in astrocytes are long-lasting in the perilesional cortex critical to brain reorganization and in turn functional recovery, astrogliosis could result in beneficial and/or harmful consequences.

Species-specific differences make it challenging to study the contribution of astrocytes to the stroke recovery process. Human astrocytes are more numerous[4] and the phenotypes of human cortical astrocytes are more complex and diverse than in their rodent counterparts.[5] Regarding stroke, human astrocytes exhibit greater susceptibility to oxidative stress compared to mouse astrocytes, due to the differences in mitochondrial physiology and detoxification pathways.[6] In addition, different signaling pathways in astrocytes are activated in response to hypoxia and inflammation between human and mouse. Because of species-specific differences in astrocytes, ischemic pathology and recovery processes are likely to be different in experimental animals and patients, which has major implications in translational research.

About 14% of stroke patients have pre-existing mild cognitive impairment or dementia.[7] Pre-existing Alzheimer's disease (AD) increases the risk of hemorrhagic stroke[8] and mortality after stroke.[9–11] Experimental studies have confirmed that coexistence of AD pathology and stroke leads to exacerbated outcomes,[12–14] possibly through activation of glial cells and upregulation of inflammatory mediators.[15] Moreover, induced pluripotent stem cell (iPSC) -derived astrocyte

progenitors from AD patients carrying AD predisposing *PSEN1* deletion in exon 9 (PSENdE9) manifest hallmarks of disease pathology, including increased β-amyloid production, altered cytokine release, and dysregulated Ca^{2+} homeostasis,[16] which all may exaggerate possible ischemic pathology.

Human glial chimeric mice offer a unique model to study how human astrocytes contribute to disease pathogenesis.[17–19] Mice transplanted with iPSC-derived astrocyte progenitors generated from patients with amyotrophic lateral sclerosis[18] and schizophrenia[20,21] show disease-related abnormal behavior suggesting an important role of astrocytes in disease progression. Here, we explored whether human iPSC-derived astrocyte progenitors transplanted in immunodeficient mice contribute to severity of stroke-related pathology and functional impairments after cortical photothrombosis. We hypothesized 1) that human astrocytes impact spontaneous sensorimotor recovery and 2) that PSEN1dE9-related astrocyte malfunctions lead to more severe ischemic damage and behavioral impairment.

MATERIALS AND METHODS

All animal procedures were approved by the Animal Ethics Committee (Hämeenlinna, Finland), and conducted in accordance with the guidelines set by the European Community Council Directives 86/609/EEC. Altogether three previously established iPSC lines were used in this study as approved by the committee on Research Ethics of Northern Savo Hospital district (license no. 123/2016).

Immunodeficient Rag1tm1Mom mutant mouse (The Jackson Laboratory) pups were transplanted on postnatal day 0 (P0) with human iPSC-astrocyte progenitors derived from AD patients (hAD) carrying PSENdE9, isogenic controls (iCTRL), a healthy donor (hCTRL), or mouse astrocytes or were injected with phosphate buffered saline (mCTRL). The health of mice was monitored by weight every third month and daily for food and water intake, general assessment of animal activity, and fur condition. At the age of 14 months, cortical ischemia was produced by intravenous Rose Bengal and cold light exposure. Behavioral outcome was assessed using behavioral tests sensitive for motor activity, sensorimotor performance, and gait before ischemia, at the acute phase, one week after ischemia, and at the end of the four weeks follow-up. After the follow-up, the mice were perfused for histology and stained for host and human astrocytes (Figure 1A). The exclusion criteria were decided before the experiment to include: 1) welfare problems before ischemia induction (e.g., injuries due to aggressive behavior) (n=10), 2) failure in transplantation or low cell survival based on missing human nuclei (HuNu)-positive cells in the cortex (n=5) and 3) no lesion based on histology (n=10). The final numbers of mice in experimental groups were: hAD (n=19), iCTRL (n=11), hCTRL (n=19), and mCTRL (n=17).

Rigor study criteria were followed. For cell transplantation, randomization was not possible, but the cells were prepared separately for each day in random order. If the litter consisted of more than nine pups, the litter was split in two and injected with two cell batches. Both female and male mice were included in the study, since at time of transplantation, sex of pups was not known. Behavioral testing was done on separate days for males and females. Surgery, all behavioral analysis, and histology were carried out in a blinded manner. Comprehensive details for all methods are provided in the Supplemental Material.

RESULTS

iPSCs differentiate into astrocytes

Correct differentiation of iPSC-derived astrocyte progenitors was analyzed immunohistochemically to confirm that the majority of cells were positive for astrocyte markers GFAP and/or aquaporin 4 (AQP4) before transplantation (Figure 1B).

Differences in body weight, infarct size, and number of transplanted cells

The welfare of mice was followed carefully after cell transplantation and atypical behavior was not observed. Body weight was measured every third month and there was a significant overall group effect *(P*<0.01) (SFigure 1A). The mCTRL group gained more weight compared to hAD (*P*<0.001) and hCTRL (*P*<0.001) mice. In addition, male mice gained more weight than females (*P*<0.001) (SFigure 1B) and there was a group x sex interaction (*P*<0.05), indicating that weight gain was different between males and females within groups.

Photothrombosis was selected for this study as it is recommended for long-term stroke recovery studies by the Stroke Recovery and Rehabilitation Roundtable Translational Working Group.[22] Induction of photothrombosis by intravenous Rose Bengal injection produced limited damage in the motor cortex, not affecting the corpus callosum (Figure 2A). After excluding mice with no lesion, infarct size was not different between groups (Figure 2B), yet female mice had overall larger ischemic damage (*P*<0.05).

Successful cell transplantation was assessed by counting HuNu-positive cells in the cortex (Figure 2C, D). No HuNu-positive cells were detected in mCTRL mice. The number of HuNu-positive cells in ipsilateral hemisphere (lesion side) was higher in mice transplanted with hAD or isogenic cells compared to mice transplanted with hCTRL cells (*P*<0.05). The number of HuNu-positive cells in the ipsilateral cortex was significantly higher compared to the contralateral cortex in the hAD group (*P*<0.05).

While HuNu-positive cells were detected widely in the brain, the cell type marker profile and identity of cells was variable. Some HuNu cells double positive with hGFAP were detected in the corpus callosum, with platelet-derived growth factor receptor alpha (PDGFRα), a marker for oligodendrocytes in the cortex, and with doublecortin (DCX), a marker for newborn neurons in the subventricular zone (SVZ) (SFigure 2).

Locomotor activity was decreased by cortical photothrombosis

Stroke-induced functional impairments were assessed using multiple sensitive behavioral tasks. Locomotor activity was measured using the open field test. At baseline, all groups showed similar locomotor activity. The distance and velocity decreased over time after photothrombosis (*P*<0.01) (Figure 3A, B). ANOVA for repeated measures also showed a significant time x group interaction (*P*<0.05) indicating time dependent differences in distance and speed among groups. Female mice were faster compared to males (*P*<0.05). Counterclockwise rotation decreased in all groups after photothrombosis (*P*<0.001) (STable 1). Counterclockwise rotation was more robust in females (*P*<0.05).

Mice prefer to spend most of their time near the walls and avoid the open center[23] and this is usually further exaggerated by cerebral ischemia. Here thigmotaxis (i.e.,time near wall) at baseline was lower in mice transplanted with human iPSC-derived astrocyte progenitors (STable 1). The time spent and frequencies of visits in the center of the open field were used as a measure of anxiety-like behavior. Indeed, mice spent most of the time near the wall, only occasionally visiting the center

zone (Figure 3C, D; STable 1). Cumulative time spent in any zone was not affected by time, group, or sex.

Minor cortical lesion produced a long-lasting impairment in sensorimotor functions but not in gait

Exploratory activity and spontaneous use of impaired (contralateral) and non-impaired (ipsilateral) forelimbs were measured by cylinder test (Figure 3E). At baseline, there were no differences between groups. There was a significant time effect ($P<0.001$) indicating persistent impairment without recovery. However, no overall group or sex effects or time interactions were observed.

Grid walking was used to assess motor coordination during locomotion. Photothrombosis induced a significant increase in number of foot-faults by impaired forelimb with slight spontaneous recovery during the follow-up ($P<0.001$) (Figure 3F). There were no differences between groups or sex or interactions with time. Behavior of non-impaired forelimbs was not affected by ischemia. Foot-faults by hindlimbs were minimal and were not counted.

CatWalk was used to characterize gait in mice. Males and females were tested separately by different detection settings to correct differences in body weight. Despite different settings, however, body weight correlated with many of the gait parameters (STable 2). Only a few scattered significant differences among groups were found at baseline (STable 2), indicating that cell transplantation itself did not affect gait. Repeated ANOVA showed a significant time effect, particularly in spatial parameters (e.g., decrease in maximum contact area after photothrombosis) (SFigure 3A, STable 3). Interestingly, there was a sex x time interaction in most of the spatial parameters for both left and right limbs. As an example, a closer examination revealed a transient decrease in maximum contact area followed by an increase only in males, which were both related to changes in body weight (SFigure 3B).

Human iPSC-derived astrocyte progenitors engrafted in the corpus callosum

We next asked whether the genotype of the transplanted astrocyte progenitors affected their overall distribution in the ischemic brain. The specificity of GFAP antibodies allowed double fluorescent stainings (SFigure 4). Whilst the transplanted human cells were scattered relatively equally throughout the brain, human GFAP positive astrocytes were located mainly in the corpus callosum (Figure 4A, B). We then measured staining intensities for ipsilateral and contralateral corpus callosum. hGFAP staining was not detected in mCRTL (Figure 5A). Ipsilateral values were higher in hAD ($P<0.01$) and hCTRL ($P<0.05$) groups. Sex did not affect the values, but interestingly, there was group x sex interaction ($P<0.05$) in both sides, possibly due to higher values in female mice.

The integrated density for host astrocytes in mCTRL was much higher compared to human astrocytes in the corpus callosum. There was also a difference between contralateral and ipsilateral sides ($P<0.001$) (Figure 5B). Values for host astrocytes in the mCTRL group were lower compared to the other groups in the contralateral side ($P<0.05$; 0.001). No significant differences were found in the ipsilateral corpus callosum. Sex did not affect the staining intensity.

Overall, the phenotype of human astrocytes (Figure 5C) was more complex compared to host ones (Figure 5E). To analyze the astrocyte phenotype in more detail, maximum intensity projections were generated from fluorescence images, converted to binary images, and skeletonized for the measurement of process lengths and endpoints (SFigure 5). There was an overall group effect in the length of processes per cell ($P<0.01$) due to the increase in hAD and iCTRL groups ($P<0.05$; $P<0.01$)

(Figure 5D).

Host astrocytes but not human astrocytes formed a glial scar

To better understand the behavioral results, we delineated a 100 μm-wide ROI at the border of the ischemic core in the cortex to measure glial responses to ischemia. Overall, integrated densities for host GFAP were much higher compared to hGFAP but were not different between the groups (Figure 6A, B, C, D). In the case of hGFAP, there was a significant overall group effect ($P<0.001$) due to lack of staining in mCTRL. mCTRL was different from hAD ($P<0.05$), iCTRL ($P<0.01$), and hCTRL ($P<0.001$) (Figure 6C). hGFAP staining intensities were higher in females ($P<0.05$).

Aβ deposits were not present in PSEN1 ΔE9 astrocyte-transplanted mice

To evaluate whether transplanted human cells produced Aβ deposits, brain sections were stained with rodent- and human-specific antibodies (SFigure 6). As positive control, sections from xxx mice were used (SFigure 6B,D). Aβ deposits were not seen in human control or PSEN1 ΔE9 astrocyte-transplanted mice. Adjacent to lesion core, rodent Aβ staining was present in all groups (SFigure 6A).

DISCUSSION

We generated chimeric mice to address for the first time how human astrocytes and astrocytic PSEN1dE9 genetic background impacted the stroke severity and outcome. Infarct size or behavioral performance was not different among experimental groups, possibly due to minimal glial scar formation by human astrocytes.

A high number of HuNu-positive transplanted cells with variable phenotypes were widely distributed in the host brain after transplantation. Although not quantified, HuNu-positive cells co-stained with hGFAP, vimentin, PDGFRα and DCX, suggesting generation of different glial cells, oligodendrocytes and neuronal progenitor phenotype. In line, Windrem et al.[20,24] showed that transplanted glial progenitors engraft and differentiate mainly into oligodendrocytes in the white matter in shiverer, myelin-deficient mice. In addition, the majority of host astrocytes are replaced by their human counterparts in shiverer mice, which was not the case in our study.

Only a low number of hGFAP positive cells were found in the cortex. One should note however, that in the healthy mouse brain GFAP content is low in cortex, subpopulations of resting astrocytes do not express the GFAP microfilament protein,[25] and GFAP immunoreactivity decreases after trauma.[26] The lack of GFAP expression does not necessarily prevent scar formation, as shown in $GFAP^{-/-}$ mice.[27] Interestingly, the majority of human GFAP-positive astrocytes remained engrafted in the corpus callosum, distant from the cortical lesion site. Moreover, the present data showed that transplanted cells with GFAP expression retain complex human astrocyte-specific morphology in the host ischemic environment, with processes being much longer in comparison to host astrocytes, in line with the previous study.[5]

Glial response to cortical photothrombosis is extensively studied in rodents.[28–30] Astrocytes are important in limiting early excitotoxicity and forming a glial scar to separate the ischemic core from surrounding healthy tissue, a scar which later secretes proteoglycans inhibiting axonal growth and regeneration in perilesional tissue.[31] We showed a strong scar formation by host astrocytes most likely due to astrocyte proliferation within the region adjacent to the lesion core. In contrast, the

number of human astrocytes was small in the perilesional cortex and their participation in glial scar formation was not observed. The reason for this may be higher susceptibility of human astrocytes to oxidative stress leading to low survival rate.[6] It may also be that human astrocytes were not activated by host ischemic signals and thus did not affect behavioral recovery as we hypothesized. Single cell RNA sequencing is needed to study further host vs. transplanted astrocyte responses to ischemic insult.

Increasing evidence suggests that cerebrovascular diseases and AD not only coexist but interact, which leads to an exacerbated outcome in experimental animals[12,14] and patients.[11,32,33] Importantly, astrocytes are implicated in both disease pathologies.[15] Of note, iPSCs derived from AD patients with pathogenic *PSEN1 ΔE9* mutation are characterized by increased Aβ1-42 production and altered cytokine release (e.g., IL-2, IL-6, IL-10) *in vitro.*[16] To our surprise, the astrocyte AD pathology did not exacerbate ischemic damage or behavioral impairment in mice, possibly due to the above discussed low number of hGFAP-positive astrocytes in the perilesional tissue. In addition, we were not able to show Aβ deposits in PSEN1 ΔE9 astrocyte-transplanted mice indicating that pathology does not spread to host tissue.

Sex-related differences exist in many aspects of stroke from epidemiology to acute treatment and outcomes.[34] The importance of using both sexes in experimental studies has been highlighted most recently by the STAIR consortium.[35] Indeed, also in our study numerous sex-specific differences were present. It is known that reproductive hormones provide natural cerebrovascular protection in women during premenopausal years.[36] After that, the rates of ischemic stroke begin to increase concomitant with the onset of menopause and loss of female sex hormones[37] and this might have contributed to the observed larger infarct volumes in females. However, although estrous cycle was not examined, mice at age of 14 months in the present study were expected to be reproductively senescent.[38] In addition, there are sex-specific differences in ischemic cell death pathways, autophagy, and immune responses.[39–41]

Our study has several technical limitations. Only iPSCs from male donors and a limited number of lines were used to keep the study design feasible. Indeed, sex-specific cellular features may lead to different responses to ischemia.[42] The observed sex-related differences in CatWalk were mainly due to body weight, which should be carefully considered in future studies.[43] The follow-up time was rather long (14 months) and transplanted cells may have retracted to quiescent state or were differentiated to oligodentrocytes.[44] Although GFAP is sensitive in detecting reactive astrocytes that respond to brain ischemia, a panel of additional astrocytic markers such S100b should have been included to assess glial phenotypes and responses more precisely.[45] Last, immunodeficient nature of the mice may confound behavioral outcomes after stroke.

In conclusion, human glial progenitor cells were transplanted into neonatal Rag1 mice generating chimeric mice to recapitulate the human condition. The survival of transplanted cells was high and cells migrated widely in the host brain after cortical photothrombosis. However, only a minority had a GFAP-positive glial phenotype, formed glial scar or impaired behavioral outcome. Caution is needed in using human glial chimeric mice in stroke research.

Acknowledgments

Nelli-Noora Välimäki carried out histological stainings, Abdulhameed Bakreen, Sara Häkli and Yannick Dunlop were responsible for behavioral testing and analysis, Hiramani Dhungana operated mice, Meike H. Keuters transplanted cells, Marja Koskuvi, Velta Keksa-Goldsteine, Minna Oksanen

and Henna Jäntti characterized and produced iPSCs and iPSC-derived astrocytes, Šárka Lehtonen, Tarja Malm, Jari Koistinaho and Jukka Jolkkonen conceived the experiment, interpreted the results, and wrote the manuscript.

Sources of Funding
This study was supported by grants from the Academy of Finland (#317866, 301234 and 328287) and Sakari and Päivikki Sohlberg foundation.

Disclosures
None.

Supplemental Materials
Expanded Material & Methods
Online Figures S1-S6
Online Tables S1-S4

REFERENCES

1. Nedergaard M, Ransom B, Goldman SA. New roles for astrocytes: redefining the functional architecture of the brain. *Trends Neurosci*. 2003;26:523–530.

2. Gleichman AJ, Carmichael ST. Astrocytic therapies for neuronal repair in stroke. *Neurosci Lett*. 2014;565:47–52.

3. Sofroniew MV. Molecular dissection of reactive astrogliosis and glial scar formation. *Trends Neurosci*. 2009;32:638–647.

4. Sherwood CC, Stimpson CD, Raghanti MA, Wildman DE, Uddin M, Grossman LI, Goodman M, Redmond JC, Bonar CJ, Erwin JM, et al. Evolution of increased glia-neuron ratios in the human frontal cortex. *Proc Natl Acad Sci U S A*. 2006;103:13606–13611.

5. Oberheim NA, Takano T, Han X, He W, Lin JHC, Wang F, Xu Q, Wyatt JD, Pilcher W, Ojemann JG, et al. Uniquely hominid features of adult human astrocytes. *J. Neurosci.* 2009;29:3276–3287.

6. Li J, Pan L, Pembroke WG, Rexach JE, Godoy MI, Condro MC, Alvarado AG, Harteni M, Chen Y-W, Stiles L, et al. Conservation and divergence of vulnerability and responses to stressors between human and mouse astrocytes. *Nat Commun*. 2021;12:3958.

7. Graber M, Garnier L, Mohr S, Delpont B, Blanc-Labarre C, Vergely C, Giroud M, Béjot Y. Influence of Pre-Existing Mild Cognitive Impairment and Dementia on Post-Stroke Mortality. The Dijon Stroke Registry. *Neuroepidemiology*. 2020;54:490–497.

8. Pinho J, Quintas-Neves M, Dogan I, Reetz K, Reich A, Costa AS. Incident stroke in patients with Alzheimer's disease: systematic review and meta-analysis. *Sci Rep*. 2021;11:16385.

9. Barba R, Morin M-M, Cemillán C, Delgado C, Domingo J, Del Ser T. Previous and incident dementia as risk factors for mortality in stroke patients. *Stroke*. 2002;33:1993–1998.

10. Desmond DW, Moroney JT, Sano M, Stern Y. Mortality in patients with dementia after ischemic stroke. *Neurology*. 2002;59:537–543.

11. Subic A, Zupanic E, von Euler M, Norrving B, Cermakova P, Religa D, Winblad B, Kramberger MG, Eriksdotter M, Garcia-Ptacek S. Stroke as a Cause of Death in Death Certificates of Patients with Dementia: A Cohort Study from the Swedish Dementia Registry. *Curr Alzheimer Res*. 2018;15:1322–1330.

12. Koistinaho M, Kettunen MI, Goldsteins G, Keinänen R, Salminen A, Ort M, Bures J, Liu D, Kauppinen RA, Higgins LS, et al. Beta-amyloid precursor protein transgenic mice that harbor diffuse A beta deposits but do not form plaques show increased ischemic vulnerability: role of inflammation. *Proc Natl Acad Sci U S A*. 2002;99:1610–1615.

13. Whitehead SN, Cheng G, Hachinski VC, Cechetto DF. Progressive increase in infarct size, neuroinflammation, and cognitive deficits in the presence of high levels of amyloid. *Stroke*. 2007;38:3245–3250.

14. Whitehead SN, Hachinski VC, Cechetto DF. Interaction between a rat model of cerebral ischemia and beta-amyloid toxicity: inflammatory responses. *Stroke*. 2005;36:107–112.

15. Koistinaho M, Koistinaho J. Interactions between Alzheimer's disease and cerebral ischemia--focus on inflammation. *Brain Res Brain Res Rev*. 2005;48:240–250.

16. Oksanen M, Petersen AJ, Naumenko N, Puttonen K, Lehtonen Š, Gubert Olivé M, Shakirzyanova A, Leskelä S, Sarajärvi T, Viitanen M, et al. PSEN1 Mutant iPSC-Derived Model Reveals Severe Astrocyte Pathology in Alzheimer's Disease. *Stem Cell Reports*. 2017;9:1885–1897.

17. Benraiss A, Wang S, Herrlinger S, Li X, Chandler-Militello D, Mauceri J, Burm HB, Toner M, Osipovitch M, Jim Xu Q, et al. Human glia can both induce and rescue aspects of disease phenotype in Huntington disease. *Nat Commun*. 2016;7:11758.

18. Chen H, Qian K, Chen W, Hu B, Blackbourn LW, Du Z, Ma L, Liu H, Knobel KM, Ayala M, et al. Human-derived neural progenitors functionally replace astrocytes in adult mice. *J Clin Invest*. 2015;125:1033–1042.

19. Goldman SA, Nedergaard M, Windrem MS. Modeling cognition and disease using human glial chimeric mice. *Glia*. 2015;63:1483–1493.

20. Windrem MS, Osipovitch M, Liu Z, Bates J, Chandler-Militello D, Zou L, Munir J, Schanz S, McCoy K, Miller RH, et al. Human iPSC Glial Mouse Chimeras Reveal Glial Contributions to Schizophrenia. *Cell Stem Cell*. 2017;21:195-208.e6.

21. Koskuvi M, Lehtonen Š, Trontti K, Keuters M, Wu Y-C, Koivisto H, Ludwig A, Plotnikova L, Virtanen PLJ, Räsänen N, et al. Contribution of astrocytes to familial risk and clinical manifestation of schizophrenia. *Glia*. 2022;70:650–660.

22. Corbett D, Carmichael ST, Murphy TH, Jones TA, Schwab ME, Jolkkonen J, Clarkson AN, Dancause N, Wieloch T, Johansen-Berg H, et al. Enhancing the alignment of the preclinical and clinical stroke recovery research pipeline: Consensus-based core recommendations from the Stroke Recovery and Rehabilitation Roundtable translational working group. *Int J Stroke*. 2017;12:462–471.

23. Lamprea MR, Cardenas FP, Setem J, Morato S. Thigmotactic responses in an open-field. *Braz J Med Biol Res*. 2008;41:135–140.

24. Windrem MS, Schanz SJ, Guo M, Tian G-F, Washco V, Stanwood N, Rasband M, Roy NS, Nedergaard M, Havton LA, et al. Neonatal Chimerization with Human Glial Progenitor Cells Can Both Remyelinate and Rescue the Otherwise Lethally Hypomyelinated Shiverer Mouse. *Cell Stem Cell*. 2008;2:553–565.

25. Kuegler PB, Baumann BA, Zimmer B, Keller S, Marx A, Kadereit S, Leist M. GFAP-independent inflammatory competence and trophic functions of astrocytes generated from murine embryonic stem cells. *Glia*. 2012;60:218–228.

26. Escartin C, Guillemaud O, Carrillo-de Sauvage M-A. Questions and (some) answers on reactive astrocytes. *Glia*. 2019;67:2221–2247.

27. Pekny M, Johansson CB, Eliasson C, Stakeberg J, Wallén Å, Perlmann T, Lendahl U, Betsholtz C, Berthold C-H, Frisén J. Abnormal Reaction to Central Nervous System Injury in Mice Lacking Glial Fibrillary Acidic Protein and Vimentin. *Journal of Cell Biology*. 1999;145:503–514.

28. Li H, Zhang N, Lin H-Y, Yu Y, Cai Q-Y, Ma L, Ding S. Histological, cellular and behavioral assessments of stroke outcomes after photothrombosis-induced ischemia in adult mice. *BMC Neurosci*. 2014;15:58.

29. Schroeter M, Schiene K, Kraemer M, Hagemann G, Weigel H, Eysel UlfT, Witte OttoW, Stoll G. Astroglial responses in photochemically induced focal ischemia of the rat cortex. *Exp Brain Res* [Internet]. 1995 [cited 2022 Jan 4];106. Available from: http://link.springer.com/10.1007/BF00241351

30. Yamaguchi A, Jitsuishi T, Hozumi T, Iwanami J, Kitajo K, Yamaguchi H, Mori Y, Mogi M, Sawai S. Temporal expression profiling of DAMPs-related genes revealed the biphasic post-ischemic inflammation in the experimental stroke model. *Mol Brain*. 2020;13:57.

31. Sims NR, Yew WP. Reactive astrogliosis in stroke: Contributions of astrocytes to recovery of neurological function. *Neurochem Int*. 2017;107:88–103.

32. Pendlebury ST, Rothwell PM. Prevalence, incidence, and factors associated with pre-stroke and post-stroke dementia: a systematic review and meta-analysis. *Lancet Neurol*. 2009;8:1006–1018.

33. Schneider JA, Arvanitakis Z, Bang W, Bennett DA. Mixed brain pathologies account for most dementia cases in community-dwelling older persons. *Neurology*. 2007;69:2197–2204.

34. Kumar A, McCullough L. Cerebrovascular disease in women. *Ther Adv Neurol Disord*. 2021;14:1756286420985237.

35. Lyden P, Buchan A, Boltze J, Fisher M, STAIR XI Consortium*. Top Priorities for Cerebroprotective Studies-A Paradigm Shift: Report From STAIR XI. *Stroke*. 2021;52:3063–3071.

36. Gibson CL. Cerebral ischemic stroke: is gender important? *J Cereb Blood Flow Metab*. 2013;33:1355–1361.

37. Towfighi A, Saver JL, Engelhardt R, Ovbiagele B. A midlife stroke surge among women in the United States. *Neurology*. 2007;69:1898–1904.

38. Frick KM. Estrogens and age-related memory decline in rodents: what have we learned and where do we go from here? *Horm Behav*. 2009;55:2–23.

39. McCullough LD, Zeng Z, Blizzard KK, Debchoudhury I, Hurn PD. Ischemic nitric oxide and poly (ADP-ribose) polymerase-1 in cerebral ischemia: male toxicity, female protection. *J Cereb Blood Flow Metab*. 2005;25:502–512.

40. Patrizz AN, Moruno-Manchon JF, O'Keefe LM, Doran SJ, Patel AR, Venna VR, Tsvetkov AS, Li J, McCullough LD. Sex-Specific Differences in Autophagic Responses to Experimental Ischemic Stroke. *Cells*. 2021;10:1825.

41. Ahnstedt H, Patrizz A, Chauhan A, Roy-O'Reilly M, Furr JW, Spychala MS, D'Aigle J, Blixt FW, Zhu L, Bravo Alegria J, et al. Sex differences in T cell immune responses, gut permeability and outcome after ischemic stroke in aged mice. *Brain Behav Immun*. 2020;87:556–567.

42. Tajiri N, Duncan K, Borlongan M, Pabon M, Acosta S, de la Pena I, Hernadez-Ontiveros D, Lozano D, Aguirre D, Reyes S, et al. Adult Stem Cell Transplantation: Is Gender a Factor in Stemness? *IJMS*. 2014;15:15225–15243.

43. Timotius IK, Bieler L, Couillard-Despres S, Sandner B, Garcia-Ovejero D, Labombarda F, Estrada V, Müller HW, Winkler J, Klucken J, et al. Combination of Defined CatWalk Gait Parameters for Predictive Locomotion Recovery in Experimental Spinal Cord Injury Rat Models. *eNeuro*. 2021;8:ENEURO.0497-20.2021.

44. Llorente IL, Hatanaka EA, Meadow ME, Xie Y, Lowry WE, Carmichael ST. Reliable generation of glial enriched progenitors from human fibroblast-derived iPSCs. *Stem Cell Research*. 2021;55:102458.

45. Escartin C, Galea E, Lakatos A, O'Callaghan JP, Petzold GC, Serrano-Pozo A, Steinhäuser C, Volterra A, Carmignoto G, Agarwal A, et al. Reactive astrocyte nomenclature, definitions, and future directions. *Nature Neuroscience*. 2021;24:312–325.

46. Chambers SM, Fasano CA, Papapetrou EP, Tomishima M, Sadelain M, Studer L. Highly efficient neural conversion of human ES and iPS cells by dual inhibition of SMAD signaling. *Nat. Biotechnol.* 2009;27:275–280.

47. Krencik R, Weick JP, Liu Y, Zhang Z-J, Zhang S-C. Specification of transplantable astroglial subtypes from human pluripotent stem cells. *Nat Biotechnol*. 2011;29:528–534.

48. Li X, Blizzard KK, Zeng Z, DeVries AC, Hurn PD, McCullough LD. Chronic behavioral testing after focal ischemia in the mouse: functional recovery and the effects of gender. *Exp Neurol*. 2004;187:94–104.

49. Clarkson AN, Huang BS, Macisaac SE, Mody I, Carmichael ST. Reducing excessive GABA-mediated tonic inhibition promotes functional recovery after stroke. *Nature*. 2010;468:305–309.

50. Young K, Morrison H. Quantifying Microglia Morphology from Photomicrographs of

Immunohistochemistry Prepared Tissue Using ImageJ. *J Vis Exp*. 2018;

FIGURE LEGENDS

Figure 1. Study design (A). Representative bright field image of astrocytes matured for 7 days and fluorescence staining for GFAP and GFAP/AQP4. Nuclei are stained with DAPI (B). Scale bar=50 μm. Figure 1A was created with BioRender.com.

Figure 2. Infarct size and human nuclei (HuNu)-positive cells in mice transplanted with hiPSC-derived astrocyte progenitors. Typical lesion location in the motor cortex from Nissl-stained section for a male (1.58 mm^3) and female (1.69 mm^3) mouse (A). Infarct size measured after behavioral follow-up was not different among experimental groups (B) but was larger in female mice (red symbols) compared to males (black symbols). HuNu-positive cells were counted from the motor cortex and were absent in mCTRL but present in the hAD, iCTRL, and hCTRL groups (C). Cell numbers were higher in ipsilateral side (D). Values are mean±S.D. Scale bar=20 μm (C). **P*<0.05 compared contralateral and ipsilateral side; #*P*<0.05 compared to hCTRL.

Figure 3. Behavioral outcome. Distance (A) and velocity (B) showed a decrease in overall activity and mobility in the open field test. Open field behavior was also used as a measure of anxiety. Mice spent most of the time near the wall, only occasionally visiting the center zone (C). Heatmap representation showed a lower activity during the follow-up (D). There were no differences among experimental groups at any time point. In the cylinder test, a significant time effect indicated persistent impairment (E). Grid walking test showed an increase in the number of forelimb foot-faults (F). Behavioral outcome was not different among experimental groups in selected tests. Values are mean±S.D. n=11-19 per group.

Figure 4. Overall distribution of host GFAP and hGFAP stained astrocytes. Low magnification image of host GFAP and hGFAP stained astrocytes in the mouse with cortical photothrombosis (A). Distribution of human and host astrocytes in the corpus callosum (B). Scale bar=10 μm (B)

Figure 5. Complex phenotype of human astrocytes in the corpus callosum. Integrated densities of human (A) and host (B) astrocytes were different in the corpus callosum. High magnification fluorescence images from the human astrocytes (C) and host astrocytes (E) in the corpus callosum. Human astrocytes had a more complex phenotype with longer processes compared to host astrocytes (D). Black symbols for males, red symbols for females. Values are mean±S.D. Scale bar=10 μm (C, E). **P*<0.05; ***P*<0.01; ****P*<0.05 compared to mCTRL group; ###*P*<0.001 compared contralateral and ipsilateral side; #*P*<0.05; ##*P*<0.01 (A, B).

Figure 6. Different behavior of host and human GFAP-positive cells in the perilesional cortex. Integrated density for host GFAP (A) and hGFAP (C) positive cells was measured in the perilesional cortex after the behavioral follow-up. Staining for host GFAP showed a strong glial scar formation around the ischemic core (B). There were no differences in the integrated density among experimental groups. Only non-specific staining for hGFAP was observed in mCTRL group. Staining pattern for hGFAP was completely different and only a few scattered hGFAP positive astrocytes were present in hAD, iCTRL, and hCTRL groups (D). White dashed line indicates lesion border. hGFAP staining

was higher in females (red symbols) (P<0.05) (B). Values are mean±S.D. Scale bar=50 μm (B1-B4, C1-C4). **P<0.01 compared to mCTRL group.

Fig. 1

A

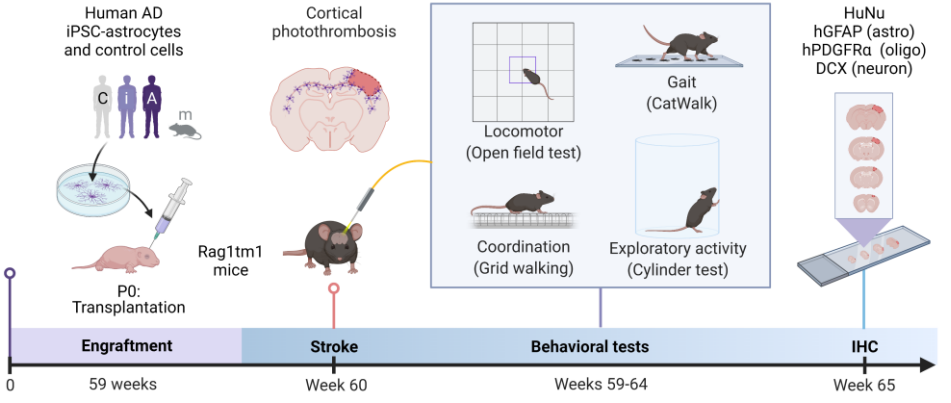

B

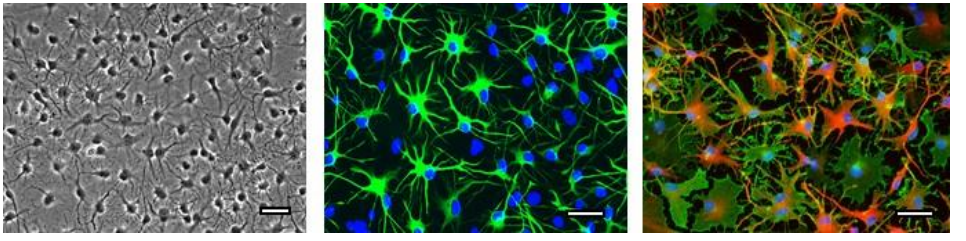

Astrocytes GFAP/DAPI AQP4/GFAP/DAPI

Fig. 2

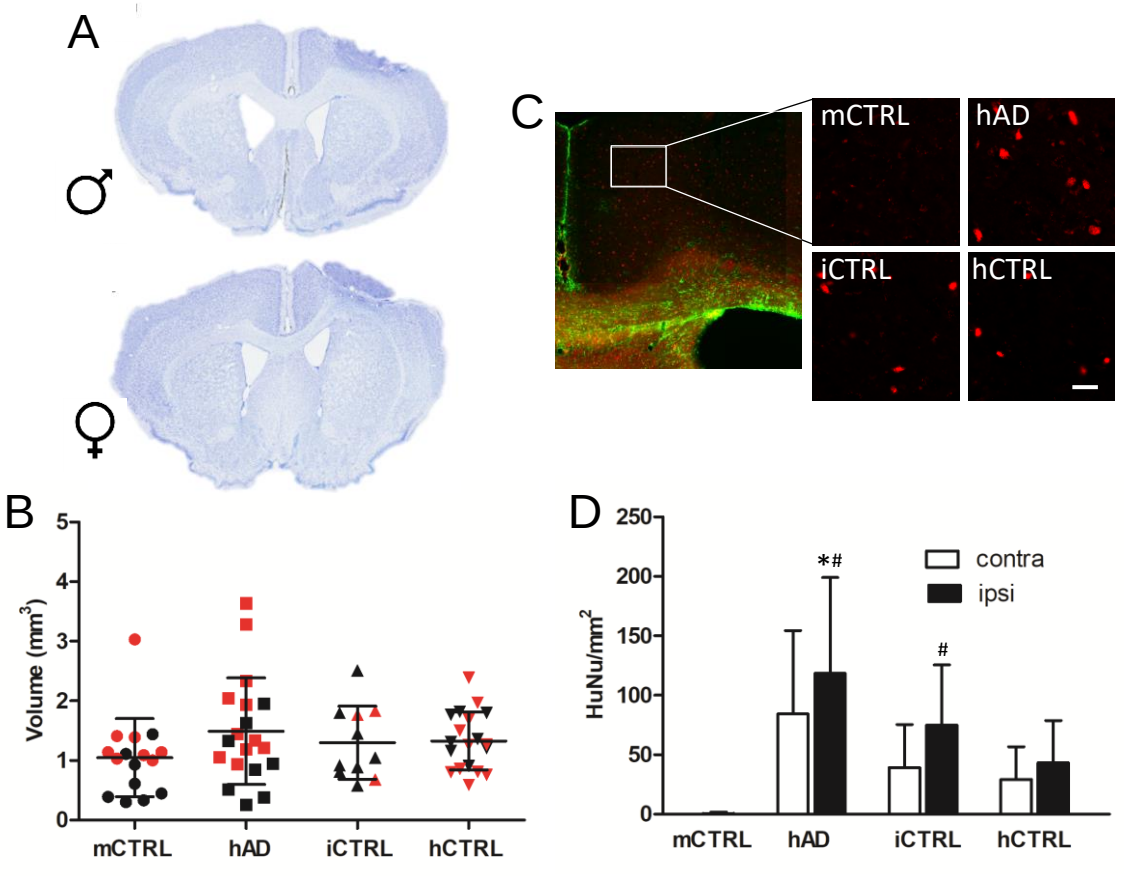
A
♂
♀
C
mCTRL
hAD
iCTRL
hCTRL
B
Volume (mm3)
0
1
2
3
4
5
mCTRL
hAD
iCTRL
hCTRL
D
HuNu/mm2
0
50
100
150
200
250
*#
#
contra
ipsi
mCTRL
hAD
iCTRL
hCTRL

Fig. 3

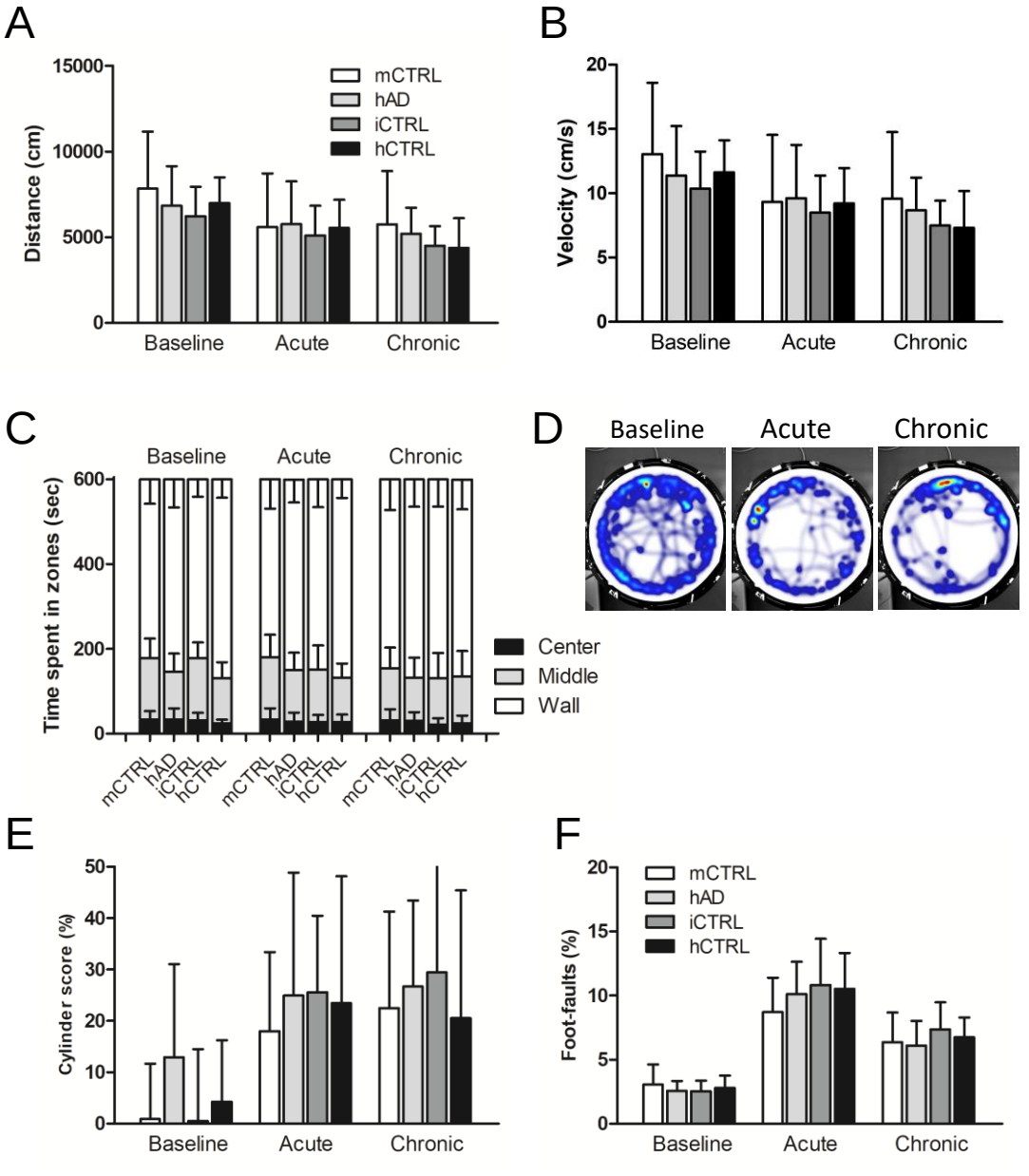
A
Distance (cm)
15000
10000
5000
0
mCTRL
hAD
iCTRL
hCTRL
Baseline
Acute
Chronic
B
Velocity (cm/s)
20
15
10
5
0
Baseline
Acute
Chronic
C
Time spent in zones (sec)
600
400
200
0
Baseline
Acute
Chronic
mCTRL
hAD
iCTRL
hCTRL
Center
Middle
Wall
D
Baseline
Acute
Chronic
E
Cylinder score (%)
50
40
30
20
10
0
Baseline
Acute
Chronic
F
Foot-faults (%)
20
15
10
5
0
mCTRL
hAD
iCTRL
hCTRL
Baseline
Acute
Chronic

Fig. 4

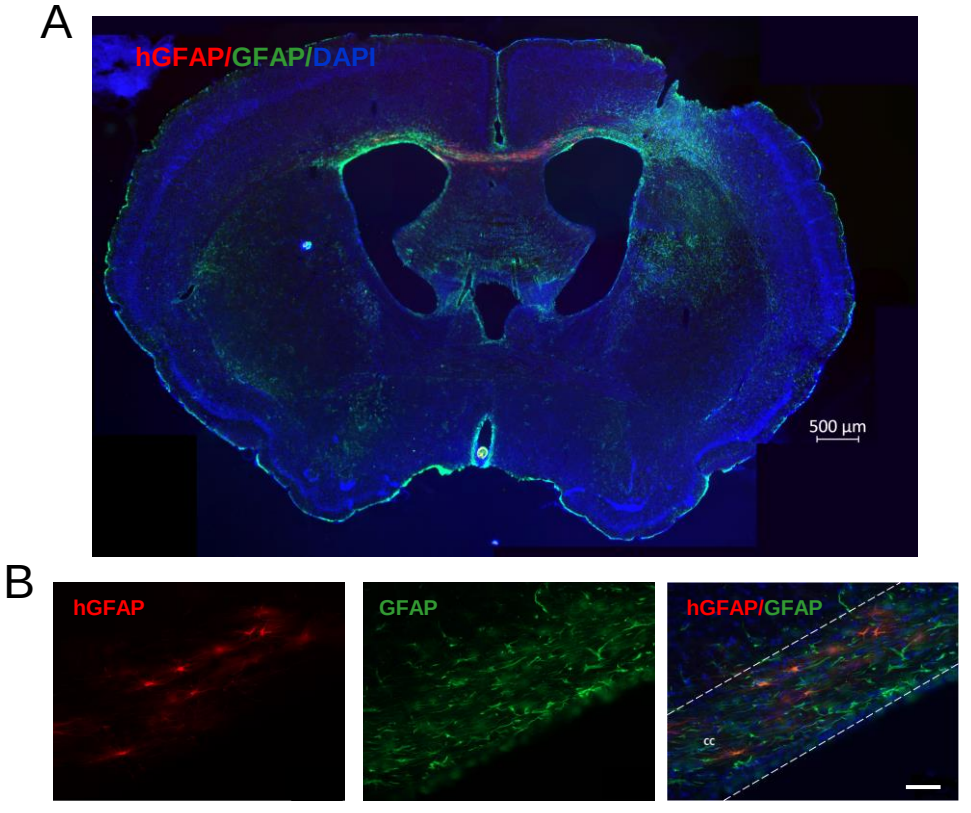

Fig. 5

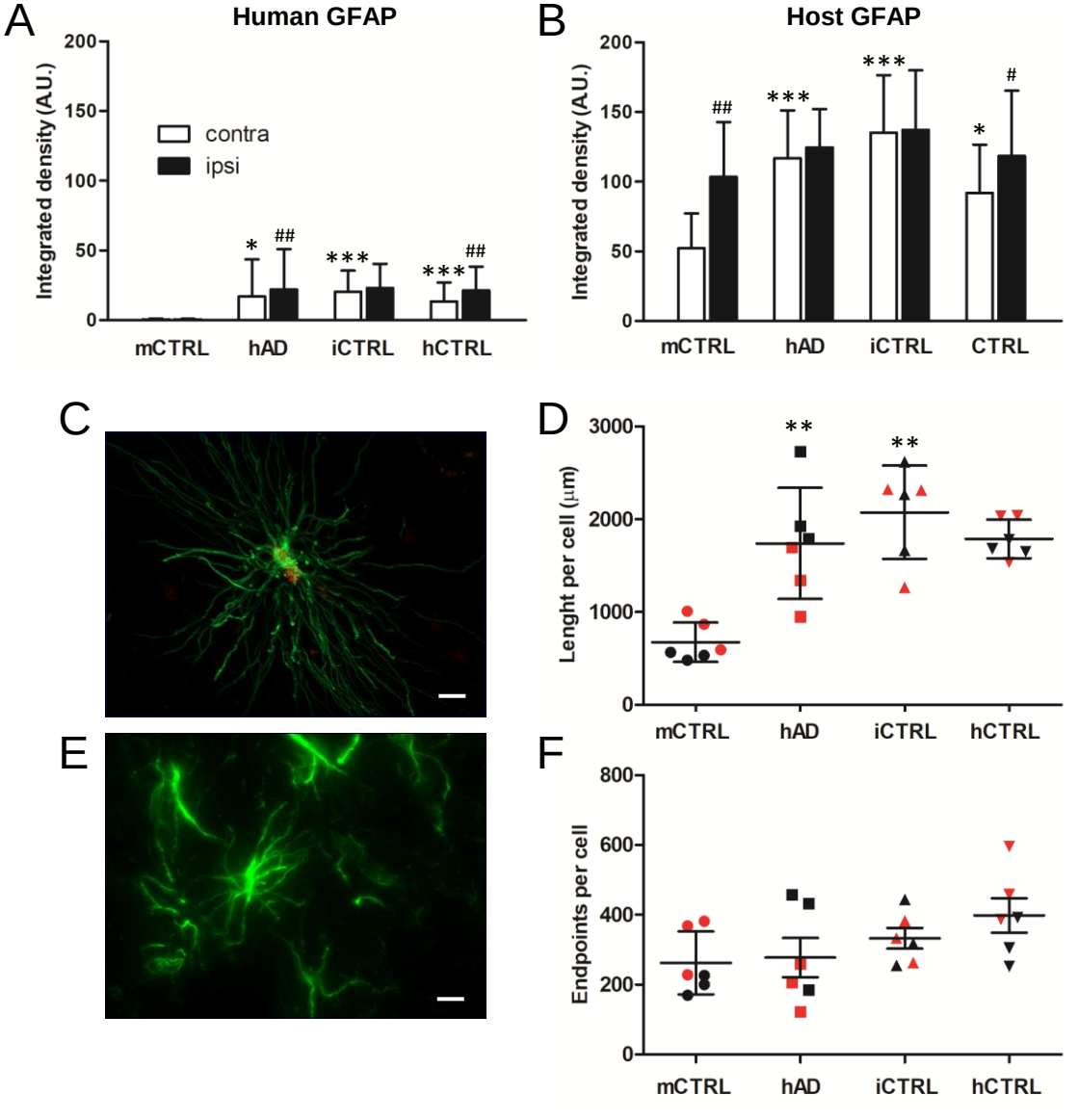
A
Human GFAP
Integrated density (AU.)
200
150
100
50
0
contra
ipsi
*
##
***
***
##
mCTRL
hAD
iCTRL
hCTRL
B
Host GFAP
Integrated density (AU.)
200
150
100
50
0
##
***
***
*
#
mCTRL
hAD
iCTRL
CTRL
C
D
Lenght per cell (µm)
3000
2000
1000
0
**
**
mCTRL
hAD
iCTRL
hCTRL
E
F
Endpoints per cell
800
600
400
200
0
mCTRL
hAD
iCTRL
hCTRL

Fig. 6

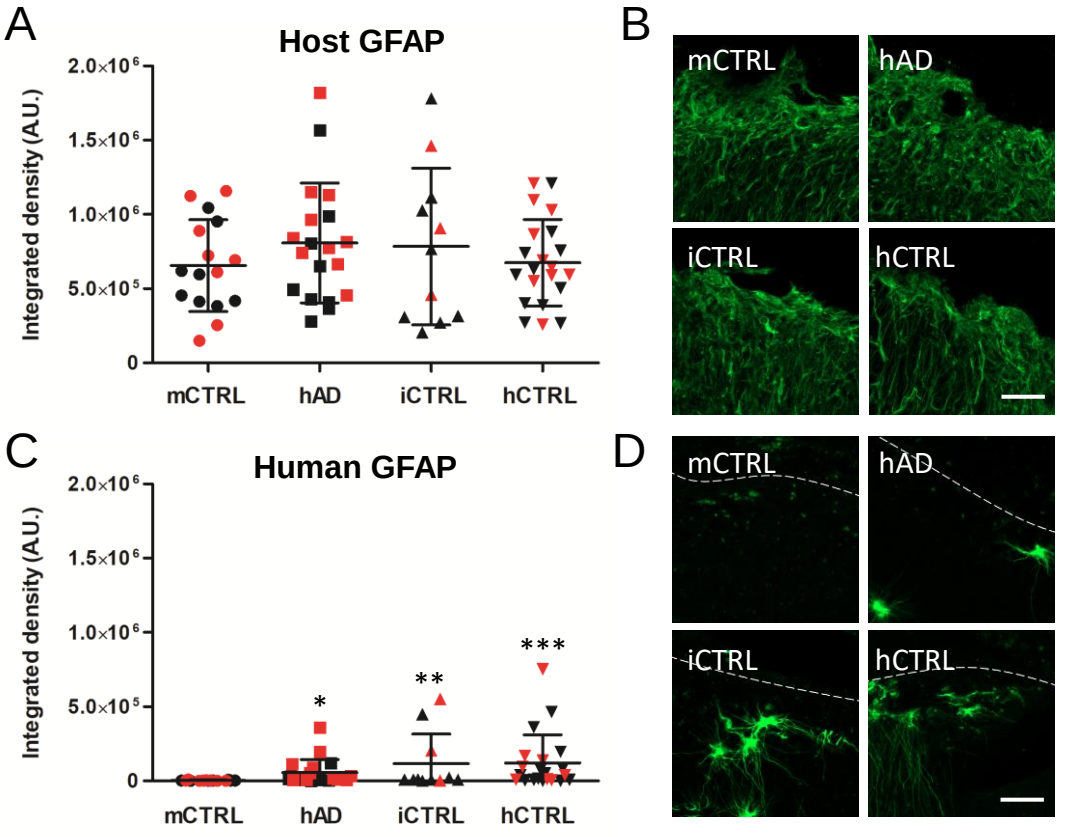
A
Host GFAP
Integrated density (A.U.)
2.0×10⁶
1.5×10⁶
1.0×10⁶
5.0×10⁵
0
mCTRL
hAD
iCTRL
hCTRL
B
mCTRL
hAD
iCTRL
hCTRL
C
Human GFAP
Integrated density (A.U.)
2.0×10⁶
1.5×10⁶
1.0×10⁶
5.0×10⁵
0
*
**
***
mCTRL
hAD
iCTRL
hCTRL
D
mCTRL
hAD
iCTRL
hCTRL

Online Figures S1-S6

Figure S1. Body weight of cell transplanted mice during the follow-up (A). Difference in body weight between female and male mice (B).

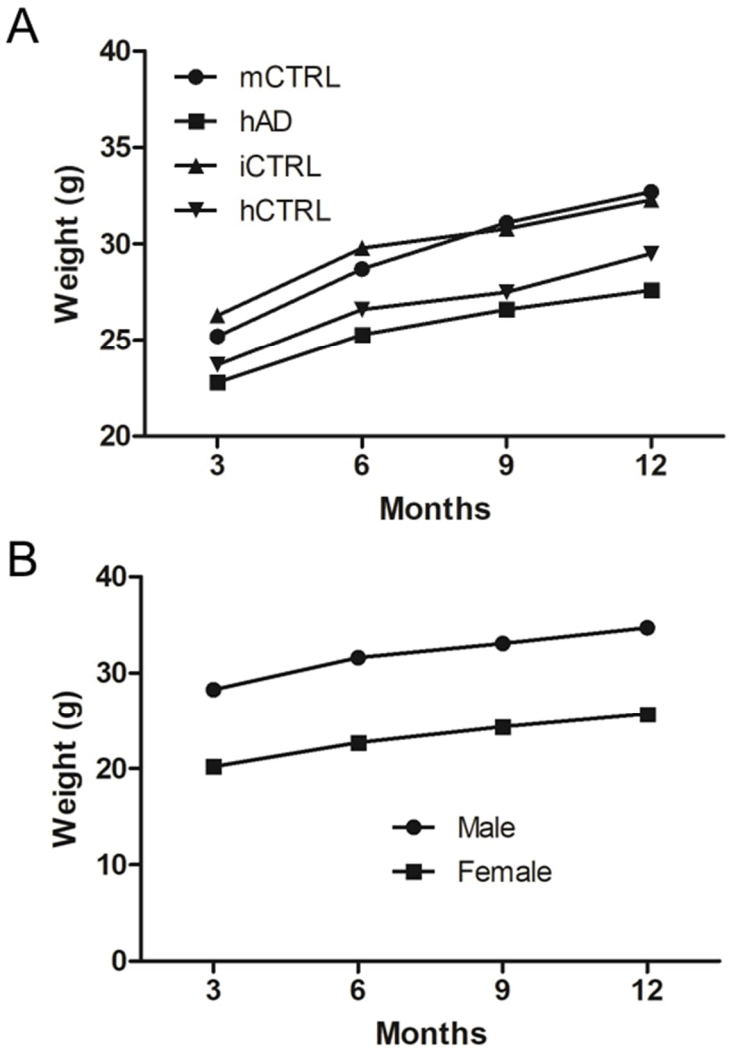

Figure S2. Phenotype of transplanted cells. Co-localization of human nuclei marker HuNu with hGFAP in the corpus callosum (A), vimentin a marker for premature astrocytes (B) and oligodendrocyte marker PDGFRα (C) in the cortex, and neurogenesis marker doublecortin (DCX) (D) in the subventricular zone. Scale bar=20 μm.

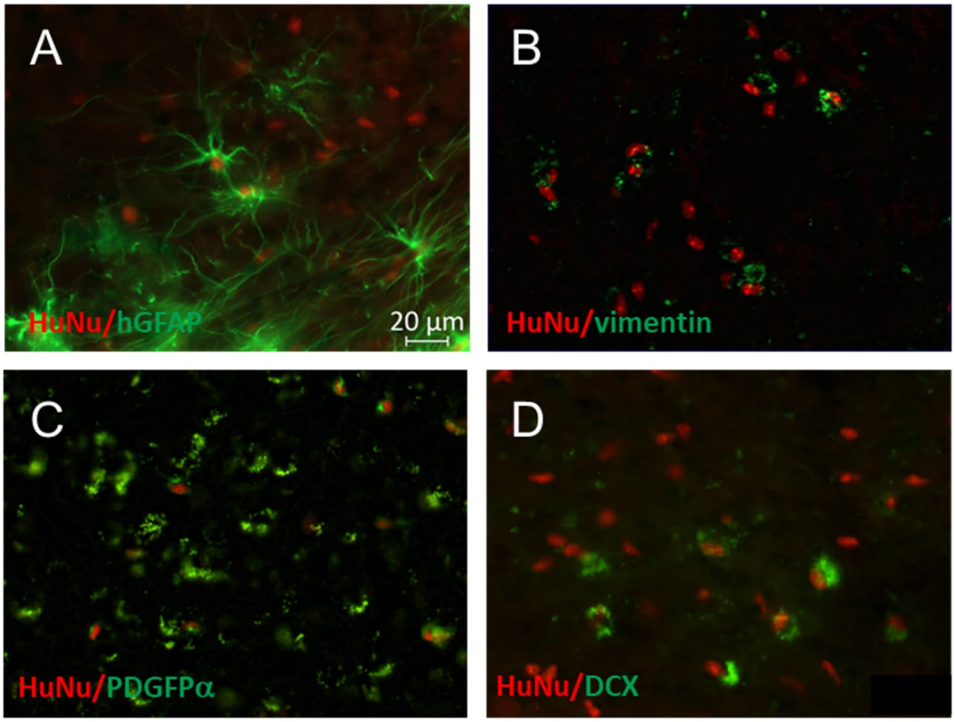

Figure S3. Maximal contact area in CatWalk among experimental groups and effect of sex.

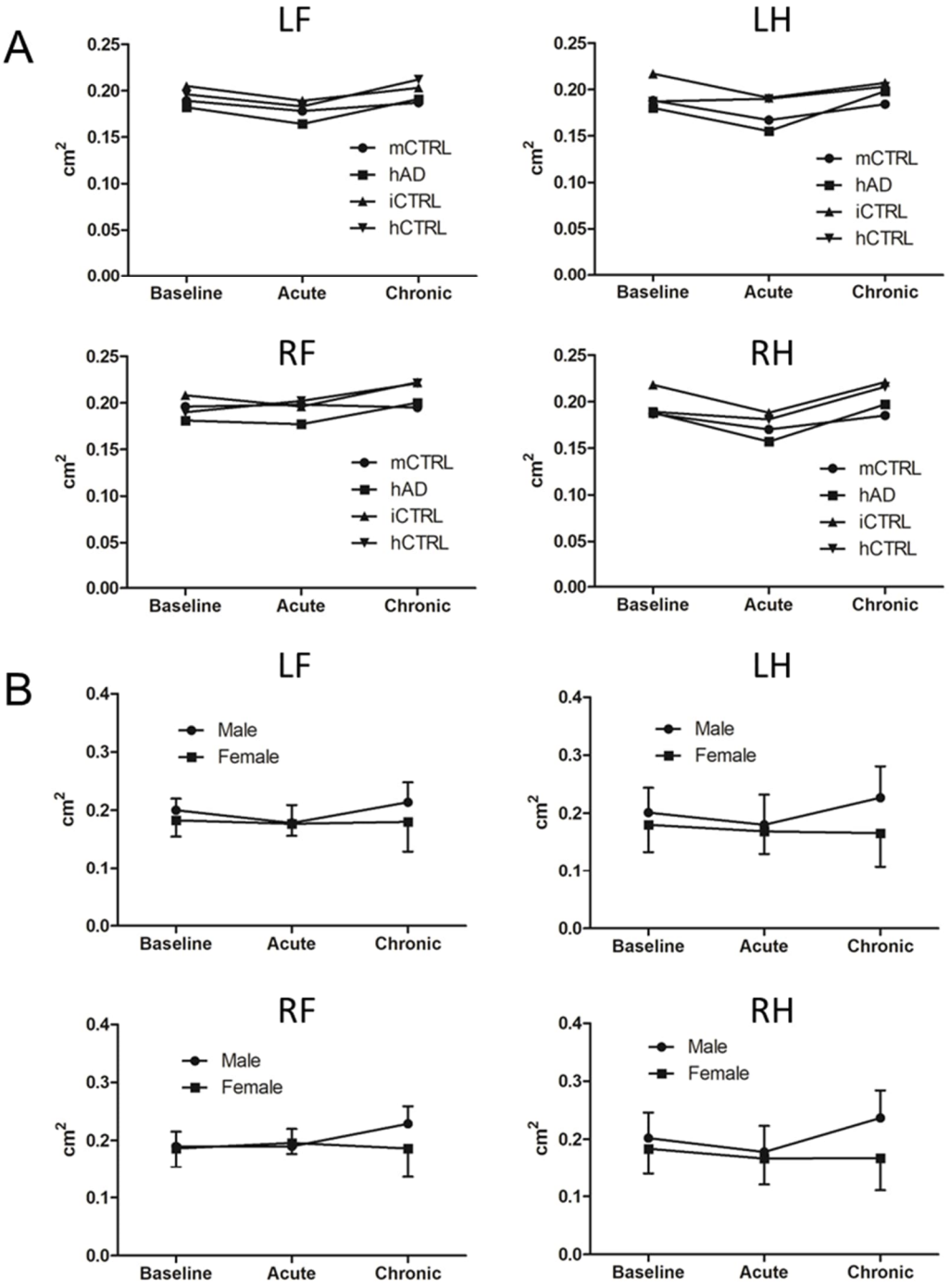

Figure S4. Specificity of GFAP antibodies used. High magnification images of human (A), host astrocytes (B) and overlay (C) in the corpus callosum. Scale bar=10 μm.

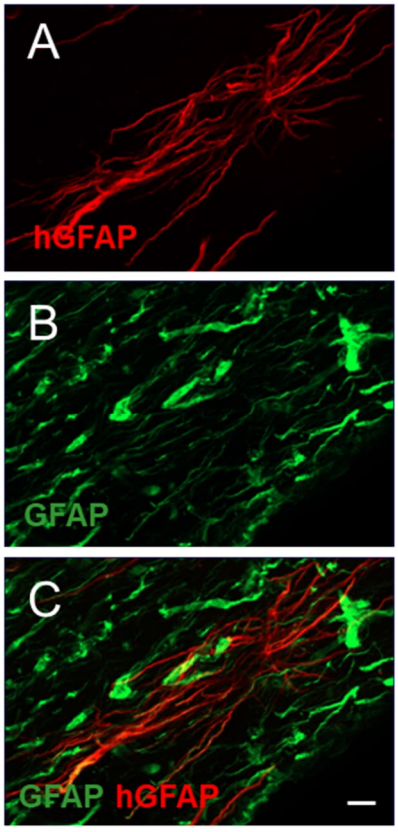

Figure S5. Fluorescence image of human astrocyte (A). Binary image skeletonized by using skeletonize function in ImageJ (B).

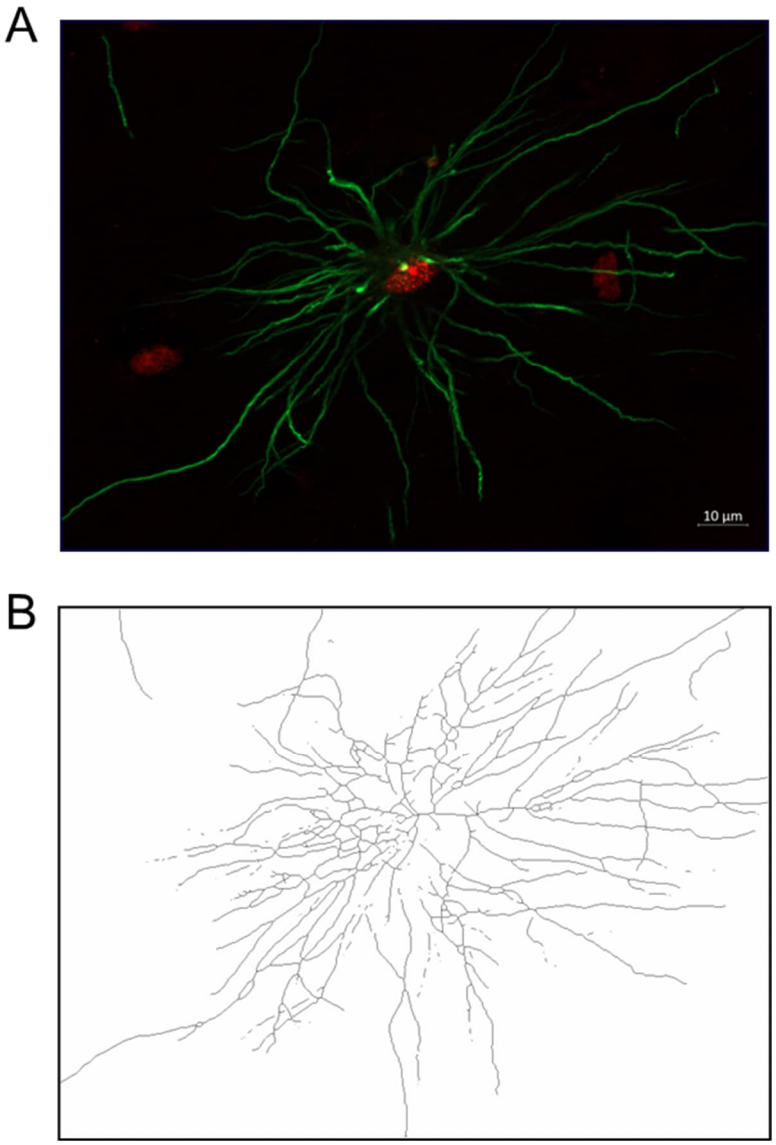

Figure S6. The representative images of rodent- (A,C) and human-specific (B,D) Aβ staining. As positive control, sections from APdE9 mouse were used (B,D). Adjacent to lesion core, rodent Aβ staining was present in all groups (A). Aβ deposits were not present in PSEN1 ΔE9 astrocyte-transplanted mouse (C).

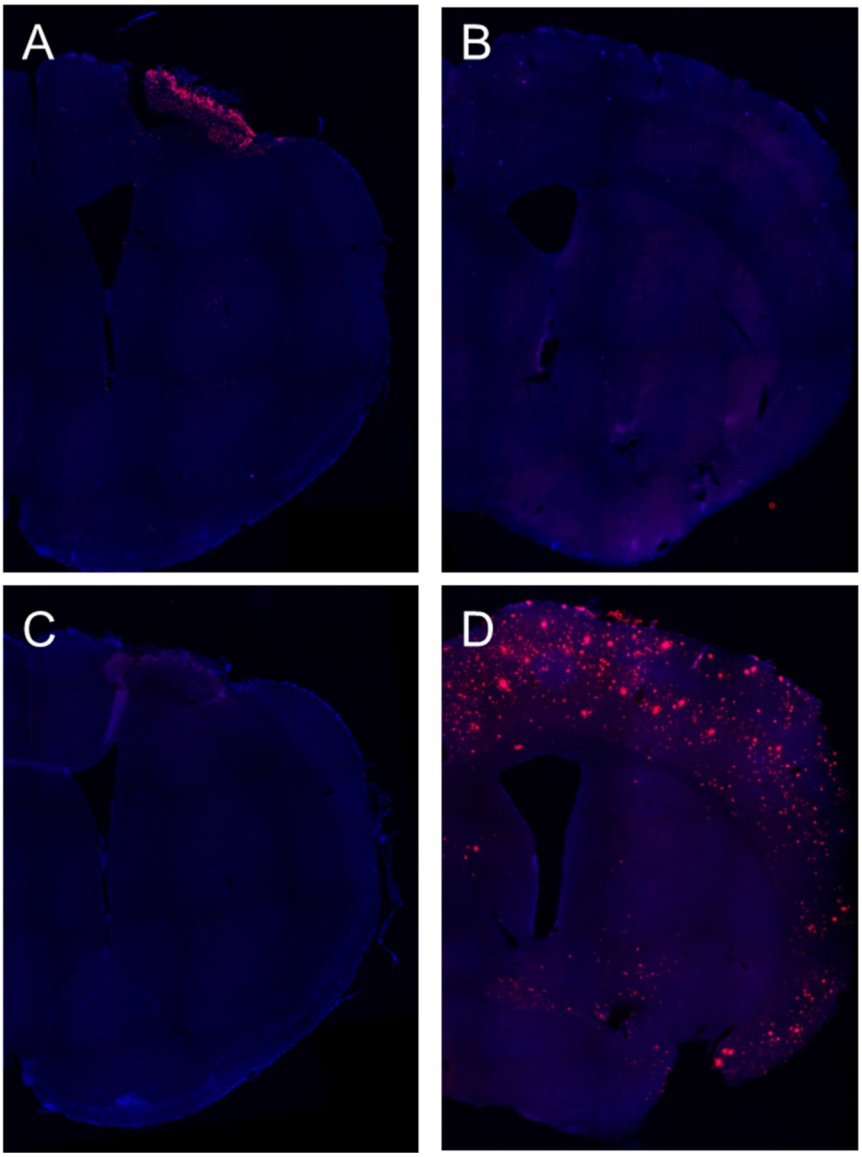

SUPPLEMENTAL MATERIAL

Astrocyte Progenitors Derived from Patients with Alzheimer's Disease Do Not Impair Stroke Recovery in Mice

Nelli-Noora Välimäki; Abdulhameed Bakreen; Sara Häkli; Hiramani Dhungana; Meike Keuters; Yannick Dunlop; Marja Koskuvi; Velta Keksa-Goldsteine; Minna Oksanen; Henna Jäntti; Šárka Lehtonen; Tarja Malm; Jari Koistinaho; Jukka Jolkkonen

Expanded Materials & Methods

Astroglial differentiation and characterization of human iPSCs

Previously established and characterized *PSEN1* exon 9 deletion (*PSEN1 ΔE9*) mutant iPSCs, their isogenic controls, and healthy donor iPSC lines were used in this study.[16] Human iPSCs were generated under the ethical approval from the Committee on Research Ethics of Northern Savo Hospital district (license no. 123/2016) and cultured in Essential 8™ Medium (E8; Thermo Fisher) as previously described.[16]

Human glial chimeric mice were generated with iPSC derived astrocyte progenitors from patients with *PSEN1 ΔE9* (n=2, AD2 clone A and B, male, 48 years), isogenic controls (n=2, generated from the same parental AD2 lines) and healthy donor (n=1, ctrl2, male, 62 years).[16]

The used astroglial differentiation protocol was modified from previously described protocols.[46,47] Briefly, the differentiation was started with human iPSCs cultured on Matrigel-coated dishes by introducing dual SMAD inhibitors 10 μM SB431542 (Sigma) and 200 nM LDN193189 (Selleckchem) for 12 days until rosette-like structure formation emerged. The cells were detached from plates and expanded in ultra-low attachment dishes (Corning) in astrocyte media consisting of DMEM/F12, 1% N2, 1% Glutamax, 0.5% penicillin/streptomycin (50 IU/50 μg/ml) (all from Invitrogen) and 0.5 IU/ml heparin (Leo Pharma) supplemented with 10ng/ml bFGF and 10 ng/ml EGF (Peprotech). Media were changed every 2-3 days and astrospheres were split manually weekly. Spheres were maintained in suspension for 5-7 months to ensure pure astroglial cultures. For astrocyte maturation, spheres were dissociated with Accutase (Stem Cell Technologies) to single cells and plated on Matrigel-coated dishes or coverslips in astrocyte medium supplemented with 10 ng/ml CNTF and 10 ng/ml BMP4 (both from Peprotech) for 7 days prior to experiments.

The dissociated astrospheres (5-7 months old) were plated and maturated for 7 days followed by characterization and transplantation. For characterization, the cells were fixed with 4 % paraformaldehyde for 20 min and further permeabilized with 0.25 % Triton X-100 in PBS (Sigma) for 1 h at room temperature (RT). After blocking with 5 % normal goat serum (Vector) in PBS at RT for 1 h, the cells were incubated with primary antibodies in PBS (GFAP, Dako, 1:500 or GFAP, Chemicon, 1:500; AQP4, Merck, 1:500) or in blocking buffer at 4 °C overnight. The second day, after washing with PBS, secondary antibodies were added (anti-rabbit Alexa Fluor 488 or anti-mouse Alexa Fluor 568, Molecular Probes, 1:300) and cells were incubated for 1 h at RT in the dark (STable 1). The cells were washed with PBS, and the nuclei were visualized with DAPI (Sigma, 1:2000, 5 min) before imaging with Zen Observer Z1 or Zen Imager AX10 (Zeiss).

Control mouse cell preparation

Neonatal mouse astrocytes were grown in DMEM (Gibco) supplemented with 10%FBS (Gibco) and 1% of penicillin/streptomycin (100 IU/100 μg/ml) (Gibco) for 10-20 days. The cells were harvested in 1.2 ml TryPLE express (Gibco) supplemented with 6 ml complete medium and centrifuged for 5 min at 400g. The pellet collected was resuspended in 1 ml PBS and filtered through a cell strainer. The cells were counted, centrifuged, and resuspended at 100 million cells/ml (= 1million/10 μl in PBS).

Procedure for cell transplantation into the brain of neonatal mice

Immunodeficient Rag1tm1Mom mutant mouse (The Jackson Laboratory) pups were transplanted on postnatal day 0 (P0). Cell suspensions (100.000 cells/µl in PBS) were prepared just before the injection. If the litter consisted of more than 9 pups, the litter was split in two and injected with two cell batches. P0 pups were anesthetized with hypothermia and fixed with the head in a stereotaxic frame (Kopf). Cell suspension (3 µl) was injected using G32 needle to the following coordinates (medial/lateral (M/L), anterior/posterior (A/P), dorsal/ventral (D/V): 0.8, 1.0, - 1.5 (0.5 µl); -0.8, 1.0, -1.5 (0.5 µl); 0.8, 2.0, -1.5 (0.5µl); -0.8, 2.0, -1.5 (0.5µl) and 0.0, -1.0 -1.5 (1µl). The rate of infusion was 0.05 µl/sec. After each injection, the needle was kept in place for 30 sec before withdrawing. The pups were placed into a 37 ^{o}C chamber with a "nest" containing material from the home cage to make sure that the dam accepted and took care of the pup after the procedure. In addition to cells from AD patients, mice were transplanted with isogenic cells, cells from healthy donor or PBS or mice astrocytes.

Cortical photothrombosis

Cortical photothrombosis was induced by photoactivation of Rose Bengal when the mice were 14 months old. Rose Bengal (Sigma) was dissolved in 0.9% NaCl in a final concentration of 15 mg/ml, filtered (Chromafil Xtra, pore size 1.20 µm), and injected into the tail vein (3.3 µl/g). Then mice were anesthetized with isoflurane (5% for induction, 2% for maintaining in 30% O_2 and 70% N_2O) and mounted to a stereotactic frame (Kopf). The skull was exposed with an approximate 1 cm incision along the midline. The cold light source was placed on the skull over the right motor cortex using the following stereotaxic coordinates: AP: +1.1 mm from Bregma; L: +2.0 mm. Ten min after Rose Bengal injection, the cold light with 3 mm aperture was switched on for 10 min (Olympus, Highlight 2100, 150 W). After the light exposure, the skin was sutured and the mice were treated for postoperative pain with Norocarp Vet (50 mg/kg, s.c., Norbrook) and a local analgesic (2% Xylocaine gel, Aspen Pharma).

Experimental groups

The final numbers of mice in experimental groups were: hAD (n=19), iCTRL (n=11), hCTRL (n=19), and mCTRL (n=17). The exclusion criteria were decided before the experiment to include: 1) welfare problems before ischemia induction (e.g., injuries due to aggressive behavior) (n=9), 2) failure in transplantation or low cell survival based on missing human nuclei (HuNu)-positive cells in the cortex (n=8) and 3) no lesion based on histology (n=11).

Table. Experimental groups.

Group	Number of mice	Males	Females	Excluded males/females
mCTRL	17	9	8	3/0
hAD	19	8	11	5/3
iCTRL	11	8	3	3/3
hCTRL	19	8	11	8/3

Behavioral testing

Behavioral testing was carried out at baseline and 1 week (acute) and 4 weeks (chronic) after ischemia. The mice were taken to corridor 30 min before testing. All behavioral tests were performed within the 12 h light cycle by an experimenter blinded to the treatment groups and in the fixed order of tests: cylinder, grid walk, open field, and CatWalk, with breaks between tests. The test devices were cleaned with 70% EtOH after each animal. Only males or females were handledduring

the test day. The mice were habituated to handling and behavioral testing beforehand.

The cylinder test was used to assess imbalance between impaired and non-impaired forelimbs.[48] For the test, the mouse was placed in a transparent cylinder (ø 11 cm) and videotaped during exploration. A camera was placed beneath the cylinder so that behavior could be filmed from below. Five min exploratory activity was analyzed by using a Kinovea program (slow speed 50%). Number of contacts on the side of the cylinder wall by both forelimb and by either impaired or nonimpaired forelimb were counted. Cylinder score for impaired forelimb was calculated as: ((nonimpaired-impaired forelimb)/(total contacts)) x 100%.

The grid-walking test was used to measure limb placement deficits and motor coordination dysfunction during locomotion. The test apparatus was made using a 12-mm square wire mesh with a grid area of 15cm length and 20 cm wide.[49] A video camera was placed beneath the grid to allow recording foot faults during a period of 3 min. The number of foot faults for each forelimb, along with the number of correct steps, were counted, and a ratio between foot faults and total steps taken was calculated: (number of foot faults/(foot faults + number of correct steps)) x 100%.

The open field test was used to measure locomotor activity and anxiety. The open field apparatusconsisted of a circular arena (ø 120 cm) surrounded by a 25 cm high wall. The location andmovement of the experimental animal were recorded by a video camera-computer linkup. Start of the test was always in the same place and in the same position of the mouse in relation to the pool. The test lasted 10 min. EthoVision XT 7.0 (Noldus, The Netherlands) was used to record and analyze the speed, distance, rotation, and time spent in three circular areas of the arena (center, middle, and wall).

CatWalk XT 9 (Noldus, The Netherlands) was used for gait analysis. The intensity threshold was set to 0.07 and the camera gain was set to 16.5 (males) and 18.8 (females) based on the average weight of tested mice. The maximum allowed speed variation was set to 50%. The testing took place underred light. Mice were allowed to run back and forth on the walkway until four uninterrupted runs were collected. During the data analysis, the steps were labeled as right forepaw (RF), right hind paw (RH), left forepaw (LF), and left hind paw (LH). Faulty labels caused by tail, whiskers, or genitalia were removed.

Perfusion

On postoperative day 33 mice were anesthetized with Equitesin (20 µl/g) and transcardially perfused with 0.9% NaCl (5 min) followed by 4% paraformaldehyde in 0.1 M PBS, pH 7.4 (9 min, 10 ml/min) (BioRad Econo Pump, 10 ml/min). The brains were carefully removed from the skull, postfixed overnight in 4% PFA at 4 ºC and cryoprotected in 30% sucrose. Brain sections (35 µm) were cut using a sliding microtome (Leica) and sections were stored in antifreeze solution at −20 °C.

Histology

The infarct size was quantified by scanning Nissl-stained sections through the lesion. Every 10th section was picked and scanned using a Hamamatsu digital slide scanner (model: C12000-02, source lens ZZ×) and measured using the Hamamatsu viewer software (NDP.view2).

Free floating sections were used for HuNu, host GFAP, human GFAP (hGFAP), platelet-derived growth factor receptor alpha (PDGFRα) and doublecortin (DCX) immunostaining. Selected sections were blocked in 10% normal goat serum. Sections for doublecortin and vimentin staining were pretreated in 0.05 M tri-sodium citrate dihydrate at pH 6.0 at 80 °C for 30 min. Mouse monoclonal anti-HuNu (1:250, Merck Millipore), rabbit polyclonal anti-GFAP (1:300, Abcam), mouse monoclonal antibody specific for human GFAP (1:500, Takara), rabbit anti-PDGFRα (1:300, Cell Signaling), rabbit polyclonal vimentin (R28) (1:1000, Cell Signaling Technology) and goat polyclonal DCX C-18 (1:500, Santa Cruz Biotechnology) were used as primary antibodies and incubated overnight at 4 ºC. Alexa Fluor goat anti-mouse 488 and 594, Alexa Fluor goat anti-rabbit 488 and Alexa Fluor donkey anti-goat 488 (1:400, Life Technologies) were used as secondary

antibodies for 2 h at RT. Sections were mounted and cover slipped with mounting medium with DAPI (Vectashield).

Additional sections were stained for rodent and human Aβ. Rodent Aβ was examined using a rodent-specific antibody (rabbit anti-rodent $A\beta_{3-16}$, SIG-39151; Covance) or a human-specific antibody (mouse anti-human $A\beta_{4-10}$, MABN10, Merck). The sections were pretreated for 30 mins with hot (85 °C) citrate buffer. Then sections were blocked in solution containing 10% Normal Goat Serum (NGS) and Tris-buffered saline with 0.5% Triton X-100 (TBS-T) for 2 h in RT. The series of sections were then transferred to a solution containing the primary antibody (rabbit anti-rodent Aβ at 1:1000 or mouse anti-human Aβ at 1:1000), 1% NGS and TBS-T at pH 8.6. After incubation in this solution overnight on a shaker table at 4 °C, the sections were rinsed three times in TBS-T and transferred to a solution containing the secondary antibody (Alexa Fluor 594 at 1:300). After 2 h incubations at RT, the sections were rinsed three times with TBS-T and once with 0.1M PB before picking up and covering the sections using mounting medium with DAPI (H-1200, Vectashield).

Table. Antibodies used in immunohistochemistry.

Type	Antibody	Origin	Manufacturer	Product
Primary	Aβ rodent	rabbit	Covance	SIG39151
	Aβ human	mouse	Merck	MABN10
	Aquaporin 4	rabbit	Merck	AB3594
	Doublecortin	goat	Santa Cruz	K1115
	GFAP	mouse	Chemicon	MAB360
	GFAP	rabbit	Dako	Z0334
	GFAP	rabbit	Abcam	AB7260
	GFAP	mouse	Takara	Y40420
	HuNu	mouse	Merck	MAB4383
	PDGFRα	rabbit	Cell Signaling Technology	5241
	Vimentin	rabbit	Cell Signaling Technology	39325
Secondary	anti-mouse 568	goat	Molecular Probes	A11004
	anti-mouse 594	goat	Life Technologies	A11032
	anti-mouse 488	goat	Life Technologies	A11029
	anti-rabbit 488	goat	Life Technologies	A11008
	anti-rabbit 488	goat	Molecular Probes	A11008

Quantification

Fluorescence images were acquired using Zeiss Axio Imager M2 with ApoTome.2. Magnification was 20x for the cortex and the corpus callosum (z-stack interval of 1 µm), 10x for perilesional cortex and 63x for individual astrocytes (z-stack interval of 0.28 µm). The number of HuNu positive cells was counted by using Fiji (ImageJ) software.

HuNu-positive cells in the ipsilateral and contralateral cortices were counted in the region of interest (ROI= $0.148mm^2$) using the automated counting of single-color images (Figure 2C). Images were first duplicated, converted to 8-bit and to grayscale. For brightness and contrast adjustment, min and max values were set to 14 and 94, respectively. Images were converted to binary by adjusting threshold to 39 and 255. Counting cells was then performed after setting the size to 200-5000 pixel^2. Masks and outlines from the analysis were then generated and compared with original images.

Integrated density was used to determine the fluorescent intensity of hGFAP staining in the corpus callosum using Fiji software. Images were first stacked with maximum intensity projection, and background was subtracted. ROIs were outlined in the ipsilateral and contralateral side and

integrated density was then measured. Two brain sections from each animal were used to retrieve the data. For host GFAP in the perilesional cortex, a specifically written macro was run to outline a 100-µm-wide area from the glial scar border, in which integrated densities were measured.

Images taken with 63x magnification from astrocytes positive for host or human GFAP were usedto receive morphological data. Skeleton analysis was done as previously described.[50] Images were first stacked with maximum intensity projection and background was subtracted. Next, the images were converted to 8-bit and grayscale before brightness and contrast were adjusted with max value set to 22. Unsharp mask and despeckle were used to further increase the contrast. Images were next converted to binaries by adjusting the threshold to 30 and 255. The quality of binary images was increased by performing functions like despeckle, close, and removing outliers with default values. Skeletonizing was performed using AnalyzeSkeleton 2D/3D plugin in ImageJ. Retrieved datasets were trimmed by measuring several fragments to first determine the cutoff value (2.0 µm), and next to cut off undesired fragments from the process length and endpoint analysis. Process lengths and endpoints were summed and divided by the number of astrocytes/somas in each image.

Statistics

Statistical analyses were performed using SPSS software for Windows (version 27). After data was checked by the Shapiro-Wilk normality test, non-parametric Kruskal-Wallis test followed by the Bonferroni *post hoc* test was used to analyze the statistical differences between groups in infarct volume, number of HuNu-positive cells, GFAP staining intensity, and astrocyte process lengths and endpoints. Mann-Whitney U test was used to analyze sex differences. Values in the ipsilateral and contralateral hemisphere were compared by Wilcoxon signed rank test. Repeated measures ANOVA with Mauchly's test of sphericity followed by the Bonferroni *post hoc* test was used for body weight and behavioral data. Correlations between body weight and CatWalk data were determined using Pearson correlation coefficients. Data are expressed as mean ± standard deviation (SD).

Online Figures S1-S6

Figure S1. Body weight of cell transplanted mice during the follow-up (A). Difference in body weight between female and male mice (B).

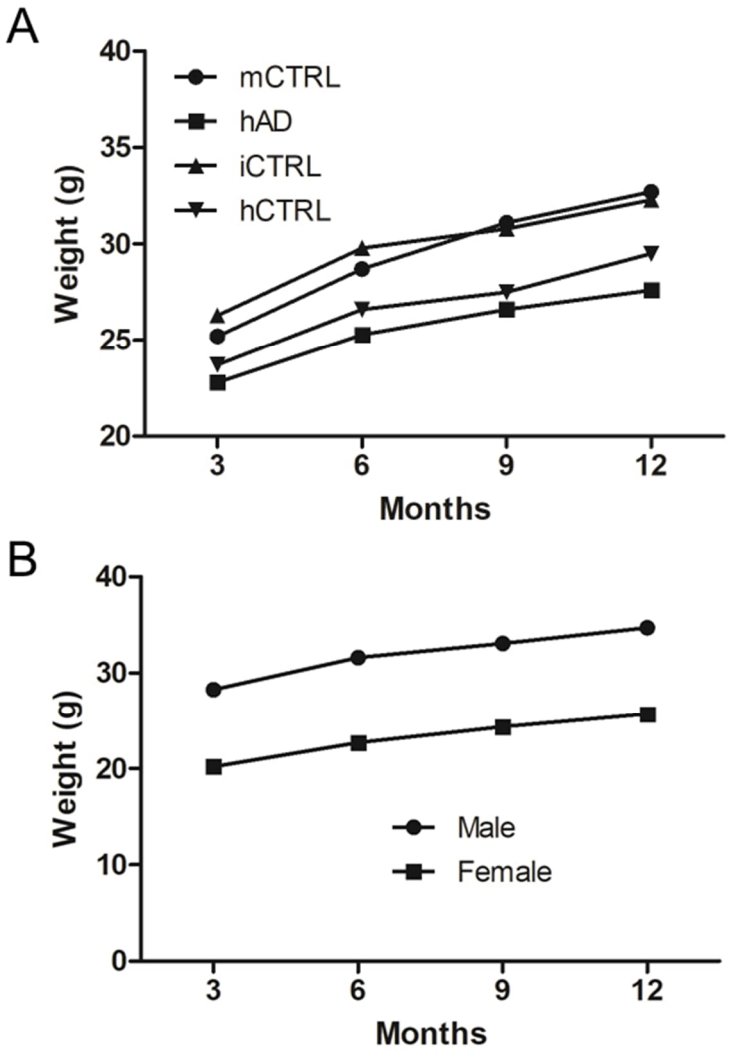

Figure S2. Phenotype of transplanted cells. Co-localization of human nuclei marker HuNu with hGFAP in the corpus callosum (A), vimentin a marker for premature astrocytes (B) and oligodendrocyte marker PDGFRα (C) in the cortex, and neurogenesis marker doublecortin (DCX) (D) in the subventricular zone. Scale bar=20 μm.

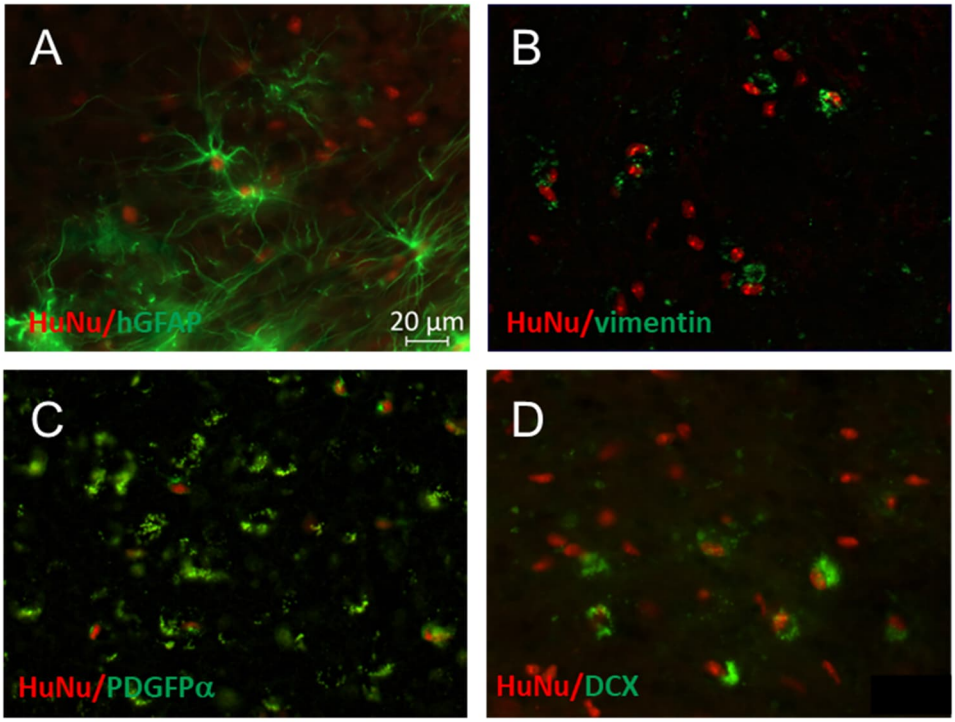

Figure S3. Maximal contact area in CatWalk among experimental groups and effect of sex.

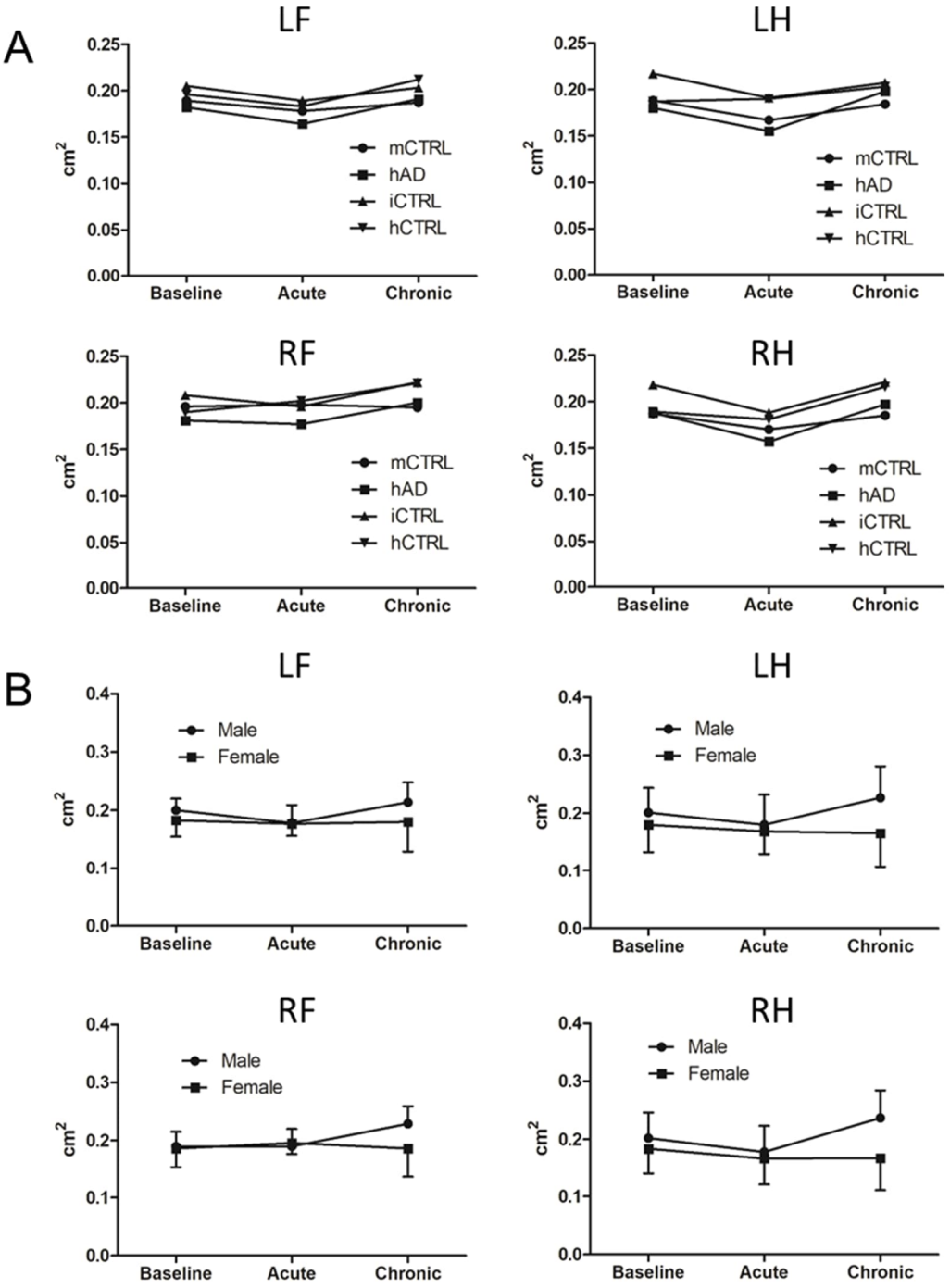

Figure S4. Specificity of GFAP antibodies used. High magnification images of human (A), host astrocytes (B) and overlay (C) in the corpus callosum. Scale bar=10 μm.

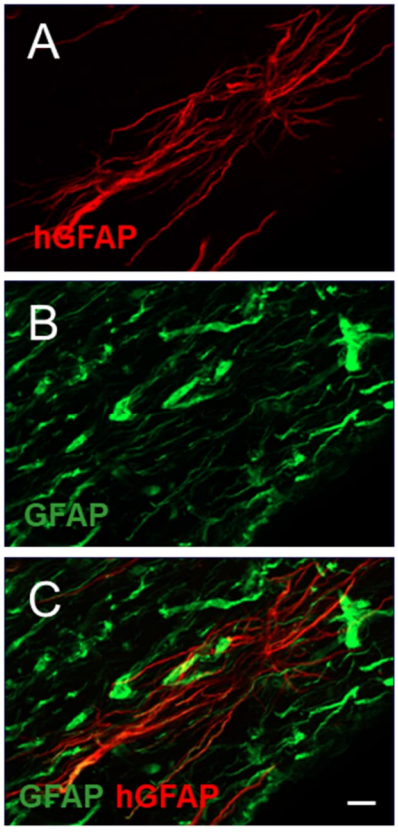

Figure S5. Fluorescence image of human astrocyte (A). Binary image skeletonized by using skeletonize function in ImageJ (B).

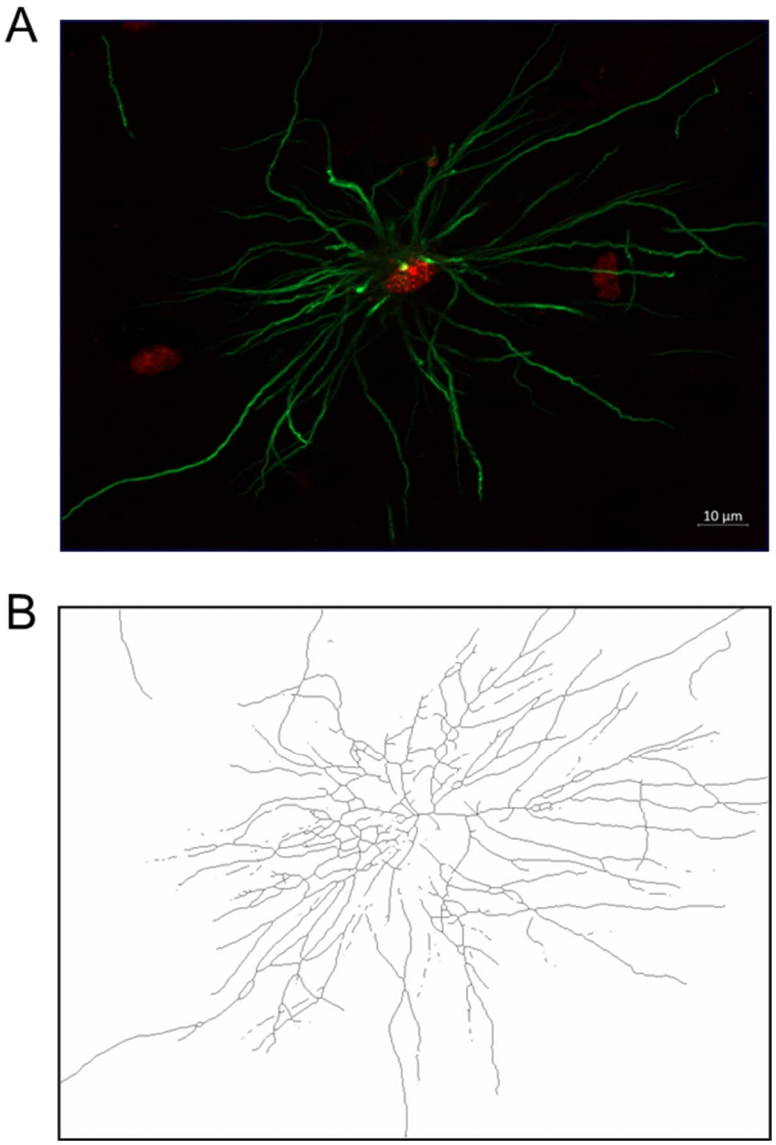

Figure S6. The representative images of rodent- (A,C) and human-specific (B,D) Aβ staining. As positive control, sections from APdE9 mouse were used (B,D). Adjacent to lesion core, rodent Aβ staining was present in all groups (A). Aβ deposits were not present in PSEN1 ΔE9 astrocyte-transplanted mouse (C).

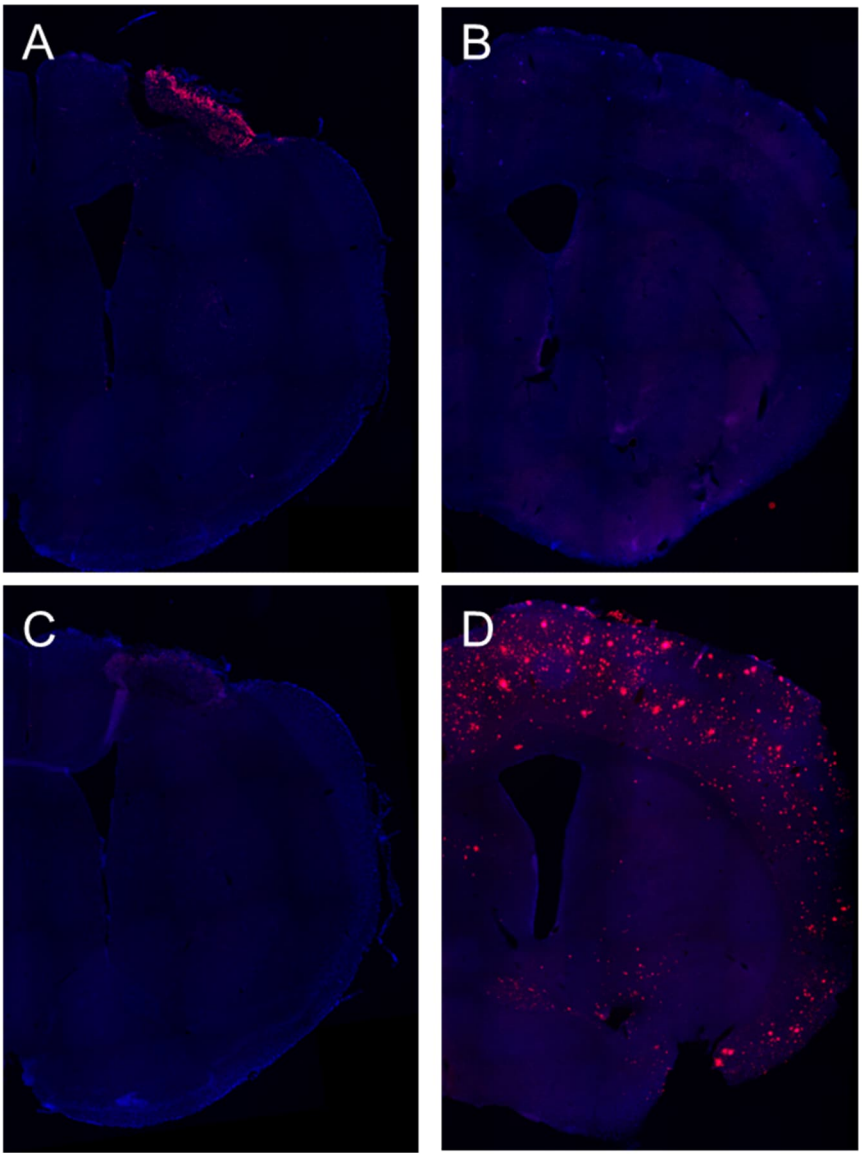

Online Tables S1-S4

Table S1. The open field data at baseline and at acute and chronic phases.

	mCTRL (n=17)	hAD (n=19)	iCTRL (n=11)	hCTRL (n=19)	ANOVA
Baseline					
Distance	7829±3324	6828±2309	6213±1731	6977±1500	0.338
Velocity	13.0±5.5	11.3±3.8	10.3±2.8	11.6±2.5	0.338
Center frequency	16.8±13.3	13.1±10.0	11.6±5.7	10.6±3.2	0.221
Center cumulative	33.1±20.2	32.9±27.0	30.9±18.3	24.6±8.3	0.528
Center latency	40.7±94.1	67.1±86.0	72.6±74.8	53.5±68.2	0.708
Wall frequency	54.2±22.1	44.9±16.2	48.1±10.1	45.5±15.7	0.356
Wall cumulative	421.5±57.5	453.9±66.2	422.2±40.8	469.2±43.4	0.032
Wall latency	4.0±6.3	0.8±2.1*	0.8±1.3	0.1±0.2**	**0.006**
Middle frequency	70.8±34.7	57.4±24.9	59.6±14.1	55.4±18.1	0.270
Middle cumulative	145.3±45.7	113.1±42.7	146.8±37.5	106.1±38.1*	**0.009**
Middle latency	6.3±8.7	9.8±14.0	4.6±8.5	7.2±10.4	0.624
Rotation cw	8.5±4.6	8.5±3.8	8.0±3.7	9.0±4.9	0.938
Ration ccw	13.4±16.0	10.7±9.0	10.0±2.3	10.5±4.1	0.753
Movement duration	488.8±68.9	471.2±65.6	463.5±84.4	491.4±49.3	0.596
Not movement duration	111.1±68.9	128.7±65.6	136.4±84.4	108.5±49.4	0.596
Acute					
Distance	5594±3128	5762±2495	5091±1738	5525±1651	0.903
Velocity	9.3±5.2	9.6±4.1	8.4±2.8	9.2±2.7	0.903
Center frequency	14.8±13.8	11.5±6.9	9.2±6.1	10.3±5.1	0.329
Center cumulative	33.4±26.3	28.7±20.9	27.1±16.8	27.0±18.0	0.803
Center latency	93.0±114.1	164.1±147.7	198.2±157.5	90.4±100.8	0.066
Wall frequency	47.6±25.7	40.8±14.8	38.5±12.3	41.3±11.1	0.508

Wall cumulative	420.0±69.6	449.9±54.0	449.0±65.5	468.3±43.9	0.108
Wall latency	0.5±1.3	0.9±2.7	0.2±0.6	0.6±1.3	0.751
Middle frequency	61.9±39.0	51.7±20.4	47.0±17.9	51.3±14.7	0.420
Middle cumulative	146.6±53.0	121.4±40.7	123.8±57.1	104.6±34.2	0.06
Middle latency	14.8±42.8	17.0±28.1	30.1±45.7	11.4±12.8	0.509
Rotation cw	4.5±3.5	4.8±3.0	4.0±2.5	6.1±2.4	0.243
Ration ccw	12.5±15.1	13.2±10.1	8.4±3.5	11.0±4.7	0.612
Movement duration	378.7±99.6	398.0±79.5	374.8±93.3	389.7±70.4	0.867
Not movement duration	221.2±99.6	201.9±79.5	225.1±93.3	210.2±70.4	0.867
Chronic					
Distance	5747±3105	5199±1521	4491±1157	4384±1721	0.199
Velocity	9.5±5.1	8.6±2.5	7.4±1.9	7.3±2.8	0.199
Center frequency	14.4±16.2	9.5±4.9	7.6±4.4	8.8±6.2	0.213
Center cumulative	31.0±26.6	29.9±20.7	20.8±16.0	24.4±18.1	0.538
Center latency	102.4±119.7	140.0±133.	139.3±141.6	179.4±107.8	0.350
Wall frequency	43.6±19.1	35.3±9.5	33.2±9.0	30.7±14.1*	**0.048**
Wall cumulative	446.1±72.2	467.8±64.8	468.4±64.0	464.9±69.9	0.755
Wall latency	0.3±0.0	0.4±1.3	0.0±01	0.1±0.6	0.593
Middle frequency	57.2±34.1	44.2±13.2	40.5±13.0	38.8±19.2	0.077
Middle cumulative	122.9±49.1	102.2±47.0	110.7±58.6	110.6±59.9	0.719
Middle latency	33.7±59.7	40.0±63.0	25.3±33.7	52.1±56.9	0.615
Rotation cw	6.2±4.7	6.4±2.8	5.6±2.4	6.3±2.5	0.929
Ration ccw	9.0±10.5	6.2±4.5	5.6±3.6	6.6±3.4	0.478
Movement duration	372.8±80.5	365.7±69.5	329.7±67.5	322.0±85.7	0.148
Not movement duration	227.1±80.5	234.2±69.5	270.2±67.5	277.9±85.5	0.148

*P<0.05; **P<0.01 (compared to mouse CTRL, Bonferroni)

Table S2. Correlations between body weight and CatWalk parameters and one-way ANOVA results at baseline and acute and chronic time points.

	correlations with body weight			**one-way ANOVA**		
	Baseline	**Acute**	**Chronic**	**Baseline**	**Acute**	**Chronic**
Run characterization						
Duration (sec)	0.147	-0.080	0.160	0.931	0.190	0.705
Temporal parameters						
RF_Stand_Mean_s	**0.370****	0.034	0.249*	0.805	0.764	0.720
LF_Stand_Mean_s	**0.319****	0.029	0.271	0.993	0.767	0.597
RH_Stand_Mean_s	**0.436*****	**0.339****	**0.400****	0.339	0.694	0.814
LH_Stand_Mean_s	**0.437*****	**0.265***	**0.418****	0.315	0.808	0.959
RF_Swing_Mean_s	-0.026	**0.482*****	**-0274***	0.998	0.824	0.395
LF_Swing_Mean_s	-0.032	-0.057	-0.054	0.680	0.680	0.995
RH_Swing_Mean_s	0.103	**-0.250***	**-0.391****	0.664	0.091	0.453
LH_Swing_Mean_s	-0.144	-0.187	**-0.346****	0.532	0.612	0.748
RF_StepCycle_Mean_s	**0.289***	**0.896*****	0.056	0.928	0.985	0.538
LF_StepCycle_Mean_s	0.199	-0.032	0.153	0.988	0.646	0.705
RH_StepCycle_Mean_s	**0.395****	**0.260***	0.151	0.643	0.980	0.995
LH_StepCycle_Mean_s	**0.341****	0.165	0.199	0.570	0.556	0.717
RF_DutyCycle_Mean_percents	**0.532*****	**0.702*****	**0.408****	0.855	0.307	0.490
LF_DutyCycle_Mean_percents	**0.333****	**0.082**	**0.294***	0.881	0.261	0.514
RH_DutyCycle_Mean_percents	**0.362****	**0.443*****	**0.526*****	0.374	0.205	0.334
LH_DutyCycle_Mean_percents	**0.459*****	**0.389****	**0.476*****	0.181	0.748	0.996
RF_SingleStance_Mean_s	0.140	**0.713*****	-0.023	0.992	0.602	0.791
LF_SingleStance_Mean_s	-0.003	0.025	-0.117	0.944	0.834	0.413
RH_SingleStance_Mean_s	-0.175	0.044	**-0.298***	0.550	0.869	0.601
LH_SingleStance_Mean_s	0.022	-0.121	-0.241	0.866	0.663	0.085
RF_InitialDualStance_Mean_s	**0.417*****	**0.715*****	**0.350****	0.934	0.227	0.977
LF_InitialDualStance_Mean_s	**0.470*****	0.118	**0.383****	0.787	0.404	0.199
RH_InitialDualStance_Mean_s	**0.547*****	**0.522*****	**0.501*****	0.146	0.936	0.691
LH_InitialDualStance_Mean_s	**0.327****	**0.273***	**0.485*****	0.361	0.507	0.958
RF_TerminalDualStance_Mean_s	**0.494*****	**0.630*****	**0.351****	0.720	0.401	0.411
LF_TerminalDualStance_Mean_s	**0.444*****	-0.018	**0.372****	0.766	0.461	0.912

RH_TerminalDualStance_Mean_s	**0.353****	**0.279***	**0.461*****	0.253	0.804	0.958
LH_TerminalDualStance_Mean_s	**0.556*****	**0.437*****	**0.480*****	0.053	0.406	0.684
RF_MaxIntensityAt_Mean_percents	**-0.418****	**0.443*****	**0.250***	0.972	0.896	0.178
LF_MaxIntensityAt_Mean_percents	0.030	**0.425*****	0.136	0.604	0.986	**0.019****
RH_MaxIntensityAt_Mean_percents	**0.285***	0.089	-0.042	0.092	0.899	0.614
LH_MaxIntensityAt_Mean_percents	0.197	-0.043	0.005	0.352	0.605	0.658
RF_MaxContactAt_Mean_percents	**-0.418*****	-0.281	**-0.361****	**0.006****	0.324	0.133
LF_MaxContactAt_Mean_percents	**-0324****	**-0.312***	-0.092	0.341	0.061	0.289
RH_MaxContactAt_Mean_percents	**0.297***	**0.251***	**-0.252***	0.295	0.336	0.262
LH_MaxContactAt_Mean_percents	**0.411****	0.150	-0.158	**0.038***	0.155	0.132
Spatial parameters						
RF_PrintLength_Mean_cm	0.222	0.072	**0.256***	0.234	0.098	0.365
LF_PrintLength_Mean_cm	**0.290***	0.028	0.167	0.245	0.420	0.327
RH_PrintLength_Mean_cm	0.209	0.181	**0.350****	0.302	0.488	0.166
LH_PrintLength_Mean_cm	**0.263***	0.105	**0.263***	**0.023***	0.061	0.906
RF_PrintWidth_Mean_cm	0.222	0.153	**0.265***	0.143	**0.018***	0.144
LF_PrintWidth_Mean_cm	**0.411****	0.016	0.136	0.108	0.428	0.485
RH_PrintWidth_Mean_cm	**0.424*****	**0.374****	**0.437****	0.281	0.536	0.641
LH_PrintWidth_Mean_cm	**0.389****	**0.464****	**0.511*****	0.084	**0.009****	0.846
RF_PrintArea_Mean_cm2	**0.258***	0.033	**0.361****	0.139	**0.046***	0.194
LF_PrintArea_Mean_cm2	**0.319****	0.148	**0.273***	0.160	0.170	0.322
RH_PrintArea_Mean_cm2	**0.312***	**0.266***	**0.479****	0.206	0.312	0.307
LH_PrintArea_Mean_cm2	**0.389****	**0.273***	**0.467*****	0.131	**0.040***	0.791
RF_MaxContactArea_Mean_sq_cm	**0.370****	0.188	**0.452*****	0.098	**0.017***	0.235
LF_MaxContactArea_Mean_sq_cm	**0.424*****	**0.341****	**0.391****	0.093	0.054	0.406
RH_MaxContactArea_Mean_sq_cm	-0.061	**0.314***	**0.527*****	0.260	0.266	0.366
LH_MaxContactArea_Mean_sq_cm	-0.094	**0.349****	**0.531*****	0.193	0.067	0.787
RF_MaxContactMaxIntensity_Mean	-0.020	**-0.427*****	0.231	0.896	0.443	0.631
LF_MaxContactMaxIntensity_Mean	-0.048	**-0.284***	0.229	0.622	0.811	0.777
RH_MaxContactMaxIntensity_Mean	0.082	0.001	0.249*	0.308	0.469	0.941
LH_MaxContactMaxIntensity_Mean	0.121	0.025	**0.294***	0.753	0.294	0.932
RF_MaxContactMeanIntensity_Mean	-0.075	**-0.514*****	**0.234**	0.939	0.799	0.686
LF_MaxContactMeanIntensity_Mean	-0.048	**-0.331****	**0.286***	0.953	0.749	0.702

RH_MaxContactMeanIntensity_Mean	-0.089	**-0.302***	0.206	0.695	0.672	0.559
LH_MaxContactMeanIntensity_Mean	-0.131	**-0.344****	0.248	0.754	0.550	0.769
RF_MaxIntensity_Mean	0.111	**-0.295***	**0.266***	0.704	0.302	0.587
LF_MaxIntensity_Mean	0.030	-0.166	0.233	0.530	0.566	0.590
RH_MaxIntensity_Mean	0.106	0.007	**0.257***	0.360	0.503	0.934
LH_MaxIntensity_Mean	0.145	0.026	**0.293***	0.710	0.259	0-935
RF_MeanIntensity_Mean	-0.024	**-0.454*****	**0.250***	0.878	0.703	0.767
LF_MeanIntensity_Mean	-0.006	**-0.286***	**0.296***	0.914	0.563	0.628
RH_MeanIntensity_Mean	-0.034	-0.220	**0.274***	0.565	0.573	0.601
LH_MeanIntensity_Mean	-0.045	-0.214	**0.332****	0.976	0.443	0.881
RF_MinIntensity_Mean	-0.010	0.086	-0.160	0.107	0.213	0.745
LF_MinIntensity_Mean	-0.007	0.030	-0.123	**0.016***	0.108	0.962
RH_MinIntensity_Mean	**-0.294***	**-0.431*****	-0.180	0.341	0.9411	0.304
LH_MinIntensity_Mean	**-0.391****	**-0.414****	**-0.262***	**0.035***	0.687	0.207
RF_MeanIntensityOfMostIntensePixels_Mean	0.090	**-0.316***	**0.329****	0.763	0.413	0.734
LF_MeanIntensityOfMostIntensePixels_Mean	0.084	-0.144	**0.331****	0.778	0.582	0.565
RH_MeanIntensityOfMostIntensePixels_Mean	0.115	-0.041	**0.320***	0.336	0.503	0.857
LH_MeanIntensityOfMostIntensePixels_Mean	0.123	0.121	**0.363****	0.874	0.250	0.916
Kinetic parameters						
RF_StandIndex_Mean	**0.345****	0.236	**0.376****	0.651	0.493	0.376
LF_StandIndex_Mean	**0.318****	0.170	**0.288***	0.894	0.926	0.858
RH_StandIndex_Mean	**0.390****	0.022	**0.422****	0.148	0.543	0.890
LH_StandIndex_Mean	**0.374****	0.068	**0.398****	**0.041***	0.556	0.431
RF_SwingSpeed_Mean_cm_per_s	0.023	**-0.644*****	-0.131	0.716	0.453	0.580
LF_SwingSpeed_Mean_cm_per_s	0.018	0.190	-0.188	0.514	0.162	0.610
RH_SwingSpeed_Mean_cm_per_s	0.094	**0.439*****	**0.258***	**0.039***	0.320	0.090
LH_SwingSpeed_Mean_cm_per_s	0.228	**0.359****	**0.331***	**0.010***	0.053	0.749
Interlimb coordination						
BOS_FrontPaws_Mean_cm	0.097	-0.104	0.046	0.460	0.769	0.677
BOS_HindPaws_Mean_cm	**0.321****	-0.141	0.172	0.376	0.452	0.149
PrintPositions_RightPaws_Mean_cm	**0.289***	-0.054	0.076	0.414	0.544	0.406
PrintPositions_LeftPaws_Mean_cm	0.101	-0.154	0.139	0.862	0.977	0.446
StepSequence_NumberOfPatterns	-0.070	0.059	0.213	0.878	0.895	0.407

StepSequence_CA_percents	-0.092	0.176	-0.132	0.267	0.822	**0.010****
StepSequence_CB_percents	0.229	0.016	0.116	0.100	0.455	0.571
StepSequence_AA_percents	-0.199	-0.001	-0.093	0.127	**0.048***	0.057
StepSequence_AB_percents	0.079	-0.064	0.133	0.151	0.153	0.948
StepSequence_RA_percents	-0.012	-0.231	0.033	0.489	0.754	0.690
StepSequence_RB_percents	0.183	-0.139	-0.127	0.172	0.555	0.175
StepSequence_RegularityIndex_percents	-0.027	**0.267***	0.005	0.670	0.445	0.155
PhaseDispersions_RF_LH_Mean	-0.171	**-0.276***	**0.258***	0.390	0.573	0.347
PhaseDispersions_LF_RH_Mean	0.006	-0.197	**0.318****	0.381	0.311	0.831
PhaseDispersions_LH_RH_Mean	0.209	0.226	0.096	0.429	0.317	**0.038***
PhaseDispersions_LF_RF_Mean	0.101	0.069	0.029	0.269	0.487	0.515
PhaseDispersions_RF_RH_Mean	0.051	0.134	0.133	0.056	0.660	0.766
PhaseDispersions_LF_LH_Mean	0.224	0.150	0.086	0.625	0.434	0.595

Table S3. Repeated ANOVA showing time effect and time x group and time x sex interactions for CatWalk parameters.

	Tests of between-subjects effects		**Tests of within-subjects effects**		
Run characterization	Group	Sex	Time	Time x Group interaction	Time x Sex interaction
Duration (sec)	0.079	0.165	0.442	0.950	0.523
Temporal parameters					
RF_Stand_Mean_s	0.371	**0.013**	0.737	0.813	0.352
LF_Stand_Mean_s	0.277	**0.026**	0.988	0.806	0.215
RH_Stand_Mean_s	0.614	**0.002**	0.132	0.604	0.906
LH_Stand_Mean_s	0.867	**0.001**	0.734	0.526	0.499
RF_Swing_Mean_s	0.681	**0.008**	0.094	0.642	**0.001**
LF_Swing_Mean_s	0.948	0.373	0.841	0.722	0.334
RH_Swing_Mean_s	0.214	**0.029**	0.193	0.722	**0.000**
LH_Swing_Mean_s	0.960	**0.020**	0.349	0.402	**0.002**
RF_StepCycle_Mean_s	0.808	0.227	0.947	0.670	0.279
LF_StepCycle_Mean_s	0.328	0.235	0.956	0.934	0.234
RH_StepCycle_Mean_s	0.958	**0.022**	0.302	0.934	0.310
LH_StepCycle_Mean_s	0.676	**0.046**	0.225	0.687	0.432
RF_DutyCycle_Mean_percents	**0.012**	**0.000**	0.145	0.748	**0.029**
LF_DutyCycle_Mean_percents	0.801	**0.000**	**0.019**	0.739	**0.010**
RH_DutyCycle_Mean_percents	0.270	**0.001**	0.070	0.709	**0.017**
LH_DutyCycle_Mean_percents	0.955	**0.000**	0.784	0.583	**0.040**
RF_SingleStance_Mean_s	0.941	0.937	0.826	0.616	0.227
LF_SingleStance_Mean_s	0.967	0.777	0.381	0.105	0.333
RH_SingleStance_Mean_s	0.930	0.459	0.118	0.553	0.201
LH_SingleStance_Mean_s	0.584	0.843	**0.000**	0.637	0.302
RF_InitialDualStance_Mean_s	0.232	**0.001**	0.713	0.782	0.246
LF_InitialDualStance_Mean_s	**0.014**	**0.000**	0.092	0.598	0.085
RH_InitialDualStance_Mean_s	0.675	**0.000**	0.494	0.710	0.515
LH_InitialDualStance_Mean_s	0.891	**0.000**	0.462	0.681	0.294

RF_TerminalDualStance_Mean_s	0.061	**0.000**	0.393	0.490	0.207
LF_TerminalDualStance_Mean_s	0.245	**0.000**	0.812	0.850	0.203
RH_TerminalDualStance_Mean_s	0.888	**0.001**	0.213	0.712	0.362
LH_TerminalDualStance_Mean_s	0.579	**0.000**	0.345	**0.045**	0.819
RF_MaxIntensityAt_Mean_percents	0.268	**0.000**	0.462	0.376	0.233
LF_MaxIntensityAt_Mean_percents	0.069	**0.000**	**0.030**	**0.040**	0.209
RH_MaxIntensityAt_Mean_percents	0.785	0.412	0.349	0.209	0.110
LH_MaxIntensityAt_Mean_percents	0.830	0.416	0.131	0.067	0.224
RF_MaxContactAt_Mean_percents	0.097	**0.025**	0.055	0.674	0.444
LF_MaxContactAt_Mean_percents	0.125	**0.012**	0.000	0.812	0.694
RH_MaxContactAt_Mean_percents	0.174	0.890	0.063	0.731	**0.004**
LH_MaxContactAt_Mean_percents	0.086	0.419	0.901	0.116	0.570
Spatial parameters					
RF_PrintLength_Mean_cm	0.264	0.519	0.692	0.100	**0.003**
LF_PrintLength_Mean_cm	0.165	0.620	0.251	0.548	**0.008**
RH_PrintLength_Mean_cm	0.317	0.058	0.317	0.517	**0.006**
LH_PrintLength_Mean_cm	0.222	0.291	0.841	0.204	**0.019**
RF_PrintWidth_Mean_cm	0.067	**0.035**	0.966	0.381	**0.001**
LF_PrintWidth_Mean_cm	0.303	0.501	0.283	0.457	**0.009**
RH_PrintWidth_Mean_cm	0.651	**0.001**	**0.017**	0.909	**0.018**
LH_PrintWidth_Mean_cm	0.288	**0.000**	0.109	0.134	**0.006**
RF_PrintArea_Mean_sq_cm	0.139	0.217	**0.023**	0.054	**0.006**
LF_PrintArea_Mean_sq_cm	0.210	0.196	**0.037**	0.206	**0.001**
RH_PrintArea_Mean_sq_cm	0.365	**0.003**	**0.007**	0.454	**0.000**
LH_PrintArea_Mean_sq_cm	0.572	0.014	**0.022**	0.114	**0.002**
RF_MaxContactArea_Mean_sq_cm	0.134	**0.007**	**0.035**	0.076	**0.000**
LF_MaxContactArea_Mean_sq_cm	0.148	**0.006**	**0.006**	0.276	**0.001**
RH_MaxContactArea_Mean_sq_cm	0.474	**0.002**	**0.001**	0.310	**0.000**
LH_MaxContactArea_Mean_sq_cm	0.335	**0.001**	**0.002**	0.160	**0.000**
RF_MaxContactMaxIntensity_Mean	0.326	0.868	**0.000**	0.551	**0.000**
LF_MaxContactMaxIntensity_Mean	0.820	0.320	**0001**	0.616	**0.000**
RH_MaxContactMaxIntensity_Mean	0.566	0.545	**0.016**	0.470	**0.000**
LH_MaxContactMaxIntensity_Mean	0.621	0.122	0.059	0.567	**0.000**

RF_MaxContactMeanIntensity_Mean	0.943	**0.000**	**0.000**	0.842	**0.009**
LF_MaxContactMeanIntensity_Mean	0.642	0.191	0.067	0.643	**0.000**
RH_MaxContactMeanIntensity_Mean	0.678	0.093	0.071	0.095	**0.000**
LH_MaxContactMeanIntensity_Mean	0.621	0.122	0.059	0.567	**0.000**
RF_MaxIntensity_Mean	0.301	0.672	**0.001**	0.714	**0.000**
LF_MaxIntensity_Mean	0.754	0.937	**0.000**	0.437	**0.000**
RH_MaxIntensity_Mean	0.699	0.118	**0.000**	0.589	**0.000**
LH_MaxIntensity_Mean	0.455	0.216	**0.000**	0.272	0.334
RF_MeanIntensity_Mean	0.678	**0.035**	0.276	0.737	**0.000**
LF_MeanIntensity_Mean	0.557	0.376	0.084	0.592	**0.000**
RH_MeanIntensity_Mean	0.660	0.405	0.733	0.108	**0.000**
LH_MeanIntensity_Mean	0.755	0.431	0.108	0.551	**0.000**
RF_MinIntensity_Mean	0.057	0.891	**0.000**	0.930	**0.005**
LF_MinIntensity_Mean	0.179	**0.001**	0.000	0.733	**0.005**
RH_MinIntensity_Mean	0.660	0.405	0.733	0.108	**0.000**
LH_MinIntensity_Mean	0.077	**0.001**	0.002	0.579	0.275
RF_MeanIntensityOfMostIntensePixels_Mean	0.556	0.541	0.171	0.492	**0.000**
LF_MeanIntensityOfMostIntensePixels_Mean	0.611	0.858	0.070	0.436	**0.000**
RH_MeanIntensityOfMostIntensePixels_Mean	0.688	0.780	**0.001**	0.226	**0.000**
LH_MeanIntensityOfMostIntensePixels_Mean	0.629	0.507	0.141	0.494	**0.000**
Kinetic parameters					
RF_StandIndex_Mean	0.521	**0.006**	0.061	0.869	0.255
LF_StandIndex_Mean	0.282	**0.027**	**0.000**	0.568	0.310
RH_StandIndex_Mean	0.760	0.098	0.234	0.141	**0.043**
LH_StandIndex_Mean	0.721	0.127	0.226	0.057	0.477
RF_SwingSpeed_Mean_cm_per_s	0.241	0.802	0.981	0.968	0.807
LF_SwingSpeed_Mean_cm_per_s	0.948	0.373	0.841	0.722	0.334
RH_SwingSpeed_Mean_cm_per_s	0.214	**0.029**	0.193	0.722	**0.000**
LH_SwingSpeed_Mean_cm_per_s	0.960	**0.020**	0.349	0.402	**0.002**
Interlimb coordination					
BOS_FrontPaws_Mean_cm	0.779	0.523	**0.016**	0.358	0.435
BOS_HindPaws_Mean_cm	0.174	0.826	0.338	0.570	**0.001**
PrintPositions_RightPaws_Mean_cm	0.577	0.585	0.920	0.487	0.218

PrintPositions_LeftPaws_Mean_cm	0.694	0.103	0.313	0.768	0.140
StepSequence_NumberOfPatterns	0.631	0.053	0.687	0.865	0.263
StepSequence_CA_percents	0.228	0.857	0.420	0.063	0.889
StepSequence_CB_percents	0.379	0.314	0.278	0.228	0.614
StepSequence_AA_percents	**0.010**	**0.015**	0.446	0.417	0.645
StepSequence_AB_percents	0.128	0.087	0.541	0.608	0.877
StepSequence_RA_percents	0.472	0.452	0.544	0.950	0.118
StepSequence_RB_percents	0.422	0.374	0.765	0.891	0.542
StepSequence_RegularityIndex_percents	0.227	**0.021**	0.081	0.832	0.067
PhaseDispersions_RF_LH_Mean	0.057	0.154	0.953	0.952	**0.008**
PhaseDispersions_LF_RH_Mean	0.293	0.662	0.985	0.732	**0.019**
PhaseDispersions_LH_RH_Mean	0.022	0.149	0.239	**0.028**	**0.039**
PhaseDispersions_LF_RF_Mean	0.697	0.928	0.941	0.110	0.619
PhaseDispersions_RF_RH_Mean	0.199	**0.006**	0.252	0.405	0.260
PhaseDispersions_LF_LH_Mean	0.067	**0.002**	0.874	0.523	0.050

Table S4. Skeleton data.

	mCTRL (n=6)	hAD (n=6)	iCTRL (n=6)	hCTRL (n=6)	ANOVA
Branch length per cell	675.5±212.4	1739.9±599.3**	2071.3±510.2***	1755.2±270.2**	*P*<0.001
End points per cell	262.4±89.7	277.3±137.3	328.3±77.8	441.2±113.4	*P*<0.05
Number of branches per cell	449.5±144.7	717.5±392.3	741.4±239.3	380.3±73.7	*P*=0.147
Number of junctions per cell	206.6±66.2	370.4±203.8	375.1±131.3	348.7±69.8	*P*=0.114
Triple points per cell	190.3±60.9	319.6±180.3	347.7±120.8	321.9±63.6	*P*=0.120
Quadrupole points per cell	15.1±4.9	30.5±25.9	25.8±11.0	24.6±6.2	*P*=0.352

**P<0.01; ***P<0.001 (compared to mouse CTRT)

Online Tables S1-S4

Table S1. The open field data at baseline and at acute and chronic phases.

	mCTRL (n=17)	hAD (n=19)	iCTRL (n=11)	hCTRL (n=19)	ANOVA
Baseline					
Distance	7829±3324	6828±2309	6213±1731	6977±1500	0.338
Velocity	13.0±5.5	11.3±3.8	10.3±2.8	11.6±2.5	0.338
Center frequency	16.8±13.3	13.1±10.0	11.6±5.7	10.6±3.2	0.221
Center cumulative	33.1±20.2	32.9±27.0	30.9±18.3	24.6±8.3	0.528
Center latency	40.7±94.1	67.1±86.0	72.6±74.8	53.5±68.2	0.708
Wall frequency	54.2±22.1	44.9±16.2	48.1±10.1	45.5±15.7	0.356
Wall cumulative	421.5±57.5	453.9±66.2	422.2±40.8	469.2±43.4	0.032
Wall latency	4.0±6.3	0.8±2.1*	0.8±1.3	0.1±0.2**	**0.006**
Middle frequency	70.8±34.7	57.4±24.9	59.6±14.1	55.4±18.1	0.270
Middle cumulative	145.3±45.7	113.1±42.7	146.8±37.5	106.1±38.1*	**0.009**
Middle latency	6.3±8.7	9.8±14.0	4.6±8.5	7.2±10.4	0.624
Rotation cw	8.5±4.6	8.5±3.8	8.0±3.7	9.0±4.9	0.938
Ration ccw	13.4±16.0	10.7±9.0	10.0±2.3	10.5±4.1	0.753
Movement duration	488.8±68.9	471.2±65.6	463.5±84.4	491.4±49.3	0.596
Not movement duration	111.1±68.9	128.7±65.6	136.4±84.4	108.5±49.4	0.596
Acute					
Distance	5594±3128	5762±2495	5091±1738	5525±1651	0.903
Velocity	9.3±5.2	9.6±4.1	8.4±2.8	9.2±2.7	0.903
Center frequency	14.8±13.8	11.5±6.9	9.2±6.1	10.3±5.1	0.329
Center cumulative	33.4±26.3	28.7±20.9	27.1±16.8	27.0±18.0	0.803
Center latency	93.0±114.1	164.1±147.7	198.2±157.5	90.4±100.8	0.066
Wall frequency	47.6±25.7	40.8±14.8	38.5±12.3	41.3±11.1	0.508

Wall cumulative	420.0±69.6	449.9±54.0	449.0±65.5	468.3±43.9	0.108
Wall latency	0.5±1.3	0.9±2.7	0.2±0.6	0.6±1.3	0.751
Middle frequency	61.9±39.0	51.7±20.4	47.0±17.9	51.3±14.7	0.420
Middle cumulative	146.6±53.0	121.4±40.7	123.8±57.1	104.6±34.2	0.06
Middle latency	14.8±42.8	17.0±28.1	30.1±45.7	11.4±12.8	0.509
Rotation cw	4.5±3.5	4.8±3.0	4.0±2.5	6.1±2.4	0.243
Ration ccw	12.5±15.1	13.2±10.1	8.4±3.5	11.0±4.7	0.612
Movement duration	378.7±99.6	398.0±79.5	374.8±93.3	389.7±70.4	0.867
Not movement duration	221.2±99.6	201.9±79.5	225.1±93.3	210.2±70.4	0.867
Chronic					
Distance	5747±3105	5199±1521	4491±1157	4384±1721	0.199
Velocity	9.5±5.1	8.6±2.5	7.4±1.9	7.3±2.8	0.199
Center frequency	14.4±16.2	9.5±4.9	7.6±4.4	8.8±6.2	0.213
Center cumulative	31.0±26.6	29.9±20.7	20.8±16.0	24.4±18.1	0.538
Center latency	102.4±119.7	140.0±133.	139.3±141.6	179.4±107.8	0.350
Wall frequency	43.6±19.1	35.3±9.5	33.2±9.0	30.7±14.1*	**0.048**
Wall cumulative	446.1±72.2	467.8±64.8	468.4±64.0	464.9±69.9	0.755
Wall latency	0.3±0.0	0.4±1.3	0.0±01	0.1±0.6	0.593
Middle frequency	57.2±34.1	44.2±13.2	40.5±13.0	38.8±19.2	0.077
Middle cumulative	122.9±49.1	102.2±47.0	110.7±58.6	110.6±59.9	0.719
Middle latency	33.7±59.7	40.0±63.0	25.3±33.7	52.1±56.9	0.615
Rotation cw	6.2±4.7	6.4±2.8	5.6±2.4	6.3±2.5	0.929
Ration ccw	9.0±10.5	6.2±4.5	5.6±3.6	6.6±3.4	0.478
Movement duration	372.8±80.5	365.7±69.5	329.7±67.5	322.0±85.7	0.148
Not movement duration	227.1±80.5	234.2±69.5	270.2±67.5	277.9±85.5	0.148

*P<0.05; **P<0.01 (compared to mouse CTRL, Bonferroni)

Table S2. Correlations between body weight and CatWalk parameters and one-way ANOVA results at baseline and acute and chronic time points.

	correlations with body weight			**one-way ANOVA**		
	Baseline	**Acute**	**Chronic**	**Baseline**	**Acute**	**Chronic**
Run characterization						
Duration (sec)	0.147	-0.080	0.160	0.931	0.190	0.705
Temporal parameters						
RF_Stand_Mean_s	**0.370****	0.034	0.249*	0.805	0.764	0.720
LF_Stand_Mean_s	**0.319****	0.029	0.271	0.993	0.767	0.597
RH_Stand_Mean_s	**0.436*****	**0.339****	**0.400****	0.339	0.694	0.814
LH_Stand_Mean_s	**0.437*****	**0.265***	**0.418****	0.315	0.808	0.959
RF_Swing_Mean_s	-0.026	**0.482*****	**-0274***	0.998	0.824	0.395
LF_Swing_Mean_s	-0.032	-0.057	-0.054	0.680	0.680	0.995
RH_Swing_Mean_s	0.103	**-0.250***	**-0.391****	0.664	0.091	0.453
LH_Swing_Mean_s	-0.144	-0.187	**-0.346****	0.532	0.612	0.748
RF_StepCycle_Mean_s	**0.289***	**0.896*****	0.056	0.928	0.985	0.538
LF_StepCycle_Mean_s	0.199	-0.032	0.153	0.988	0.646	0.705
RH_StepCycle_Mean_s	**0.395****	**0.260***	0.151	0.643	0.980	0.995
LH_StepCycle_Mean_s	**0.341****	0.165	0.199	0.570	0.556	0.717
RF_DutyCycle_Mean_percents	**0.532*****	**0.702*****	**0.408****	0.855	0.307	0.490
LF_DutyCycle_Mean_percents	**0.333****	**0.082**	**0.294***	0.881	0.261	0.514
RH_DutyCycle_Mean_percents	**0.362****	**0.443*****	**0.526*****	0.374	0.205	0.334
LH_DutyCycle_Mean_percents	**0.459*****	**0.389****	**0.476*****	0.181	0.748	0.996
RF_SingleStance_Mean_s	0.140	**0.713*****	-0.023	0.992	0.602	0.791
LF_SingleStance_Mean_s	-0.003	0.025	-0.117	0.944	0.834	0.413
RH_SingleStance_Mean_s	-0.175	0.044	**-0.298***	0.550	0.869	0.601
LH_SingleStance_Mean_s	0.022	-0.121	-0.241	0.866	0.663	0.085
RF_InitialDualStance_Mean_s	**0.417*****	**0.715*****	**0.350****	0.934	0.227	0.977
LF_InitialDualStance_Mean_s	**0.470*****	0.118	**0.383****	0.787	0.404	0.199
RH_InitialDualStance_Mean_s	**0.547*****	**0.522*****	**0.501*****	0.146	0.936	0.691
LH_InitialDualStance_Mean_s	**0.327****	**0.273***	**0.485*****	0.361	0.507	0.958
RF_TerminalDualStance_Mean_s	**0.494*****	**0.630*****	**0.351****	0.720	0.401	0.411
LF_TerminalDualStance_Mean_s	**0.444*****	-0.018	**0.372****	0.766	0.461	0.912

RH_TerminalDualStance_Mean_s	**0.353****	**0.279***	**0.461*****	0.253	0.804	0.958
LH_TerminalDualStance_Mean_s	**0.556*****	**0.437*****	**0.480*****	0.053	0.406	0.684
RF_MaxIntensityAt_Mean_percents	**-0.418****	**0.443*****	**0.250***	0.972	0.896	0.178
LF_MaxIntensityAt_Mean_percents	0.030	**0.425*****	0.136	0.604	0.986	**0.019****
RH_MaxIntensityAt_Mean_percents	**0.285***	0.089	-0.042	0.092	0.899	0.614
LH_MaxIntensityAt_Mean_percents	0.197	-0.043	0.005	0.352	0.605	0.658
RF_MaxContactAt_Mean_percents	**-0.418*****	-0.281	**-0.361****	**0.006****	0.324	0.133
LF_MaxContactAt_Mean_percents	**-0324****	**-0.312***	-0.092	0.341	0.061	0.289
RH_MaxContactAt_Mean_percents	**0.297***	**0.251***	**-0.252***	0.295	0.336	0.262
LH_MaxContactAt_Mean_percents	**0.411****	0.150	-0.158	**0.038***	0.155	0.132
Spatial parameters						
RF_PrintLength_Mean_cm	0.222	0.072	**0.256***	0.234	0.098	0.365
LF_PrintLength_Mean_cm	**0.290***	0.028	0.167	0.245	0.420	0.327
RH_PrintLength_Mean_cm	0.209	0.181	**0.350****	0.302	0.488	0.166
LH_PrintLength_Mean_cm	**0.263***	0.105	**0.263***	**0.023***	0.061	0.906
RF_PrintWidth_Mean_cm	0.222	0.153	**0.265***	0.143	**0.018***	0.144
LF_PrintWidth_Mean_cm	**0.411****	0.016	0.136	0.108	0.428	0.485
RH_PrintWidth_Mean_cm	**0.424*****	**0.374****	**0.437****	0.281	0.536	0.641
LH_PrintWidth_Mean_cm	**0.389****	**0.464****	**0.511*****	0.084	**0.009****	0.846
RF_PrintArea_Mean_cm2	**0.258***	0.033	**0.361****	0.139	**0.046***	0.194
LF_PrintArea_Mean_cm2	**0.319****	0.148	**0.273***	0.160	0.170	0.322
RH_PrintArea_Mean_cm2	**0.312***	**0.266***	**0.479****	0.206	0.312	0.307
LH_PrintArea_Mean_cm2	**0.389****	**0.273***	**0.467*****	0.131	**0.040***	0.791
RF_MaxContactArea_Mean_sq_cm	**0.370****	0.188	**0.452*****	0.098	**0.017***	0.235
LF_MaxContactArea_Mean_sq_cm	**0.424*****	**0.341****	**0.391****	0.093	0.054	0.406
RH_MaxContactArea_Mean_sq_cm	-0.061	**0.314***	**0.527*****	0.260	0.266	0.366
LH_MaxContactArea_Mean_sq_cm	-0.094	**0.349****	**0.531*****	0.193	0.067	0.787
RF_MaxContactMaxIntensity_Mean	-0.020	**-0.427*****	0.231	0.896	0.443	0.631
LF_MaxContactMaxIntensity_Mean	-0.048	**-0.284***	0.229	0.622	0.811	0.777
RH_MaxContactMaxIntensity_Mean	0.082	0.001	0.249*	0.308	0.469	0.941
LH_MaxContactMaxIntensity_Mean	0.121	0.025	**0.294***	0.753	0.294	0.932
RF_MaxContactMeanIntensity_Mean	-0.075	**-0.514*****	**0.234**	0.939	0.799	0.686
LF_MaxContactMeanIntensity_Mean	-0.048	**-0.331****	**0.286***	0.953	0.749	0.702

RH_MaxContactMeanIntensity_Mean	-0.089	**-0.302***	0.206	0.695	0.672	0.559
LH_MaxContactMeanIntensity_Mean	-0.131	**-0.344****	0.248	0.754	0.550	0.769
RF_MaxIntensity_Mean	0.111	**-0.295***	**0.266***	0.704	0.302	0.587
LF_MaxIntensity_Mean	0.030	-0.166	0.233	0.530	0.566	0.590
RH_MaxIntensity_Mean	0.106	0.007	**0.257***	0.360	0.503	0.934
LH_MaxIntensity_Mean	0.145	0.026	**0.293***	0.710	0.259	0-935
RF_MeanIntensity_Mean	-0.024	**-0.454*****	**0.250***	0.878	0.703	0.767
LF_MeanIntensity_Mean	-0.006	**-0.286***	**0.296***	0.914	0.563	0.628
RH_MeanIntensity_Mean	-0.034	-0.220	**0.274***	0.565	0.573	0.601
LH_MeanIntensity_Mean	-0.045	-0.214	**0.332****	0.976	0.443	0.881
RF_MinIntensity_Mean	-0.010	0.086	-0.160	0.107	0.213	0.745
LF_MinIntensity_Mean	-0.007	0.030	-0.123	**0.016***	0.108	0.962
RH_MinIntensity_Mean	**-0.294***	**-0.431*****	-0.180	0.341	0.9411	0.304
LH_MinIntensity_Mean	**-0.391****	**-0.414****	**-0.262***	**0.035***	0.687	0.207
RF_MeanIntensityOfMostIntensePixels_Mean	0.090	**-0.316***	**0.329****	0.763	0.413	0.734
LF_MeanIntensityOfMostIntensePixels_Mean	0.084	-0.144	**0.331****	0.778	0.582	0.565
RH_MeanIntensityOfMostIntensePixels_Mean	0.115	-0.041	**0.320***	0.336	0.503	0.857
LH_MeanIntensityOfMostIntensePixels_Mean	0.123	0.121	**0.363****	0.874	0.250	0.916
Kinetic parameters						
RF_StandIndex_Mean	**0.345****	0.236	**0.376****	0.651	0.493	0.376
LF_StandIndex_Mean	**0.318****	0.170	**0.288***	0.894	0.926	0.858
RH_StandIndex_Mean	**0.390****	0.022	**0.422****	0.148	0.543	0.890
LH_StandIndex_Mean	**0.374****	0.068	**0.398****	**0.041***	0.556	0.431
RF_SwingSpeed_Mean_cm_per_s	0.023	**-0.644*****	-0.131	0.716	0.453	0.580
LF_SwingSpeed_Mean_cm_per_s	0.018	0.190	-0.188	0.514	0.162	0.610
RH_SwingSpeed_Mean_cm_per_s	0.094	**0.439*****	**0.258***	**0.039***	0.320	0.090
LH_SwingSpeed_Mean_cm_per_s	0.228	**0.359****	**0.331***	**0.010***	0.053	0.749
Interlimb coordination						
BOS_FrontPaws_Mean_cm	0.097	-0.104	0.046	0.460	0.769	0.677
BOS_HindPaws_Mean_cm	**0.321****	-0.141	0.172	0.376	0.452	0.149
PrintPositions_RightPaws_Mean_cm	**0.289***	-0.054	0.076	0.414	0.544	0.406
PrintPositions_LeftPaws_Mean_cm	0.101	-0.154	0.139	0.862	0.977	0.446
StepSequence_NumberOfPatterns	-0.070	0.059	0.213	0.878	0.895	0.407

StepSequence_CA_percents	-0.092	0.176	-0.132	0.267	0.822	**0.010****
StepSequence_CB_percents	0.229	0.016	0.116	0.100	0.455	0.571
StepSequence_AA_percents	-0.199	-0.001	-0.093	0.127	**0.048***	0.057
StepSequence_AB_percents	0.079	-0.064	0.133	0.151	0.153	0.948
StepSequence_RA_percents	-0.012	-0.231	0.033	0.489	0.754	0.690
StepSequence_RB_percents	0.183	-0.139	-0.127	0.172	0.555	0.175
StepSequence_RegularityIndex_percents	-0.027	**0.267***	0.005	0.670	0.445	0.155
PhaseDispersions_RF_LH_Mean	-0.171	**-0.276***	**0.258***	0.390	0.573	0.347
PhaseDispersions_LF_RH_Mean	0.006	-0.197	**0.318****	0.381	0.311	0.831
PhaseDispersions_LH_RH_Mean	0.209	0.226	0.096	0.429	0.317	**0.038***
PhaseDispersions_LF_RF_Mean	0.101	0.069	0.029	0.269	0.487	0.515
PhaseDispersions_RF_RH_Mean	0.051	0.134	0.133	0.056	0.660	0.766
PhaseDispersions_LF_LH_Mean	0.224	0.150	0.086	0.625	0.434	0.595

Table S3. Repeated ANOVA showing time effect and time x group and time x sex interactions for CatWalk parameters.

	Tests of between-subjects effects		**Tests of within-subjects effects**		
Run characterization	Group	Sex	Time	Time x Group interaction	Time x Sex interaction
Duration (sec)	0.079	0.165	0.442	0.950	0.523
Temporal parameters					
RF_Stand_Mean_s	0.371	**0.013**	0.737	0.813	0.352
LF_Stand_Mean_s	0.277	**0.026**	0.988	0.806	0.215
RH_Stand_Mean_s	0.614	**0.002**	0.132	0.604	0.906
LH_Stand_Mean_s	0.867	**0.001**	0.734	0.526	0.499
RF_Swing_Mean_s	0.681	**0.008**	0.094	0.642	**0.001**
LF_Swing_Mean_s	0.948	0.373	0.841	0.722	0.334
RH_Swing_Mean_s	0.214	**0.029**	0.193	0.722	**0.000**
LH_Swing_Mean_s	0.960	**0.020**	0.349	0.402	**0.002**
RF_StepCycle_Mean_s	0.808	0.227	0.947	0.670	0.279
LF_StepCycle_Mean_s	0.328	0.235	0.956	0.934	0.234
RH_StepCycle_Mean_s	0.958	**0.022**	0.302	0.934	0.310
LH_StepCycle_Mean_s	0.676	**0.046**	0.225	0.687	0.432
RF_DutyCycle_Mean_percents	**0.012**	**0.000**	0.145	0.748	**0.029**
LF_DutyCycle_Mean_percents	0.801	**0.000**	**0.019**	0.739	**0.010**
RH_DutyCycle_Mean_percents	0.270	**0.001**	0.070	0.709	**0.017**
LH_DutyCycle_Mean_percents	0.955	**0.000**	0.784	0.583	**0.040**
RF_SingleStance_Mean_s	0.941	0.937	0.826	0.616	0.227
LF_SingleStance_Mean_s	0.967	0.777	0.381	0.105	0.333
RH_SingleStance_Mean_s	0.930	0.459	0.118	0.553	0.201
LH_SingleStance_Mean_s	0.584	0.843	**0.000**	0.637	0.302
RF_InitialDualStance_Mean_s	0.232	**0.001**	0.713	0.782	0.246
LF_InitialDualStance_Mean_s	**0.014**	**0.000**	0.092	0.598	0.085
RH_InitialDualStance_Mean_s	0.675	**0.000**	0.494	0.710	0.515
LH_InitialDualStance_Mean_s	0.891	**0.000**	0.462	0.681	0.294

RF_TerminalDualStance_Mean_s	0.061	**0.000**	0.393	0.490	0.207
LF_TerminalDualStance_Mean_s	0.245	**0.000**	0.812	0.850	0.203
RH_TerminalDualStance_Mean_s	0.888	**0.001**	0.213	0.712	0.362
LH_TerminalDualStance_Mean_s	0.579	**0.000**	0.345	**0.045**	0.819
RF_MaxIntensityAt_Mean_percents	0.268	**0.000**	0.462	0.376	0.233
LF_MaxIntensityAt_Mean_percents	0.069	**0.000**	**0.030**	**0.040**	0.209
RH_MaxIntensityAt_Mean_percents	0.785	0.412	0.349	0.209	0.110
LH_MaxIntensityAt_Mean_percents	0.830	0.416	0.131	0.067	0.224
RF_MaxContactAt_Mean_percents	0.097	**0.025**	0.055	0.674	0.444
LF_MaxContactAt_Mean_percents	0.125	**0.012**	0.000	0.812	0.694
RH_MaxContactAt_Mean_percents	0.174	0.890	0.063	0.731	**0.004**
LH_MaxContactAt_Mean_percents	0.086	0.419	0.901	0.116	0.570
Spatial parameters					
RF_PrintLength_Mean_cm	0.264	0.519	0.692	0.100	**0.003**
LF_PrintLength_Mean_cm	0.165	0.620	0.251	0.548	**0.008**
RH_PrintLength_Mean_cm	0.317	0.058	0.317	0.517	**0.006**
LH_PrintLength_Mean_cm	0.222	0.291	0.841	0.204	**0.019**
RF_PrintWidth_Mean_cm	0.067	**0.035**	0.966	0.381	**0.001**
LF_PrintWidth_Mean_cm	0.303	0.501	0.283	0.457	**0.009**
RH_PrintWidth_Mean_cm	0.651	**0.001**	**0.017**	0.909	**0.018**
LH_PrintWidth_Mean_cm	0.288	**0.000**	0.109	0.134	**0.006**
RF_PrintArea_Mean_sq_cm	0.139	0.217	**0.023**	0.054	**0.006**
LF_PrintArea_Mean_sq_cm	0.210	0.196	**0.037**	0.206	**0.001**
RH_PrintArea_Mean_sq_cm	0.365	**0.003**	**0.007**	0.454	**0.000**
LH_PrintArea_Mean_sq_cm	0.572	0.014	**0.022**	0.114	**0.002**
RF_MaxContactArea_Mean_sq_cm	0.134	**0.007**	**0.035**	0.076	**0.000**
LF_MaxContactArea_Mean_sq_cm	0.148	**0.006**	**0.006**	0.276	**0.001**
RH_MaxContactArea_Mean_sq_cm	0.474	**0.002**	**0.001**	0.310	**0.000**
LH_MaxContactArea_Mean_sq_cm	0.335	**0.001**	**0.002**	0.160	**0.000**
RF_MaxContactMaxIntensity_Mean	0.326	0.868	**0.000**	0.551	**0.000**
LF_MaxContactMaxIntensity_Mean	0.820	0.320	**0001**	0.616	**0.000**
RH_MaxContactMaxIntensity_Mean	0.566	0.545	**0.016**	0.470	**0.000**
LH_MaxContactMaxIntensity_Mean	0.621	0.122	0.059	0.567	**0.000**

RF_MaxContactMeanIntensity_Mean	0.943	**0.000**	**0.000**	0.842	**0.009**
LF_MaxContactMeanIntensity_Mean	0.642	0.191	0.067	0.643	**0.000**
RH_MaxContactMeanIntensity_Mean	0.678	0.093	0.071	0.095	**0.000**
LH_MaxContactMeanIntensity_Mean	0.621	0.122	0.059	0.567	**0.000**
RF_MaxIntensity_Mean	0.301	0.672	**0.001**	0.714	**0.000**
LF_MaxIntensity_Mean	0.754	0.937	**0.000**	0.437	**0.000**
RH_MaxIntensity_Mean	0.699	0.118	**0.000**	0.589	**0.000**
LH_MaxIntensity_Mean	0.455	0.216	**0.000**	0.272	0.334
RF_MeanIntensity_Mean	0.678	**0.035**	0.276	0.737	**0.000**
LF_MeanIntensity_Mean	0.557	0.376	0.084	0.592	**0.000**
RH_MeanIntensity_Mean	0.660	0.405	0.733	0.108	**0.000**
LH_MeanIntensity_Mean	0.755	0.431	0.108	0.551	**0.000**
RF_MinIntensity_Mean	0.057	0.891	**0.000**	0.930	**0.005**
LF_MinIntensity_Mean	0.179	**0.001**	0.000	0.733	**0.005**
RH_MinIntensity_Mean	0.660	0.405	0.733	0.108	**0.000**
LH_MinIntensity_Mean	0.077	**0.001**	0.002	0.579	0.275
RF_MeanIntensityOfMostIntensePixels_Mean	0.556	0.541	0.171	0.492	**0.000**
LF_MeanIntensityOfMostIntensePixels_Mean	0.611	0.858	0.070	0.436	**0.000**
RH_MeanIntensityOfMostIntensePixels_Mean	0.688	0.780	**0.001**	0.226	**0.000**
LH_MeanIntensityOfMostIntensePixels_Mean	0.629	0.507	0.141	0.494	**0.000**
Kinetic parameters					
RF_StandIndex_Mean	0.521	**0.006**	0.061	0.869	0.255
LF_StandIndex_Mean	0.282	**0.027**	**0.000**	0.568	0.310
RH_StandIndex_Mean	0.760	0.098	0.234	0.141	**0.043**
LH_StandIndex_Mean	0.721	0.127	0.226	0.057	0.477
RF_SwingSpeed_Mean_cm_per_s	0.241	0.802	0.981	0.968	0.807
LF_SwingSpeed_Mean_cm_per_s	0.948	0.373	0.841	0.722	0.334
RH_SwingSpeed_Mean_cm_per_s	0.214	**0.029**	0.193	0.722	**0.000**
LH_SwingSpeed_Mean_cm_per_s	0.960	**0.020**	0.349	0.402	**0.002**
Interlimb coordination					
BOS_FrontPaws_Mean_cm	0.779	0.523	**0.016**	0.358	0.435
BOS_HindPaws_Mean_cm	0.174	0.826	0.338	0.570	**0.001**
PrintPositions_RightPaws_Mean_cm	0.577	0.585	0.920	0.487	0.218

PrintPositions_LeftPaws_Mean_cm	0.694	0.103	0.313	0.768	0.140
StepSequence_NumberOfPatterns	0.631	0.053	0.687	0.865	0.263
StepSequence_CA_percents	0.228	0.857	0.420	0.063	0.889
StepSequence_CB_percents	0.379	0.314	0.278	0.228	0.614
StepSequence_AA_percents	**0.010**	**0.015**	0.446	0.417	0.645
StepSequence_AB_percents	0.128	0.087	0.541	0.608	0.877
StepSequence_RA_percents	0.472	0.452	0.544	0.950	0.118
StepSequence_RB_percents	0.422	0.374	0.765	0.891	0.542
StepSequence_RegularityIndex_percents	0.227	**0.021**	0.081	0.832	0.067
PhaseDispersions_RF_LH_Mean	0.057	0.154	0.953	0.952	**0.008**
PhaseDispersions_LF_RH_Mean	0.293	0.662	0.985	0.732	**0.019**
PhaseDispersions_LH_RH_Mean	0.022	0.149	0.239	**0.028**	**0.039**
PhaseDispersions_LF_RF_Mean	0.697	0.928	0.941	0.110	0.619
PhaseDispersions_RF_RH_Mean	0.199	**0.006**	0.252	0.405	0.260
PhaseDispersions_LF_LH_Mean	0.067	**0.002**	0.874	0.523	0.050

Table S4. Skeleton data.

	mCTRL (n=6)	hAD (n=6)	iCTRL (n=6)	hCTRL (n=6)	ANOVA
Branch length per cell	675.5±212.4	1739.9±599.3**	2071.3±510.2***	1755.2±270.2**	*P*<0.001
End points per cell	262.4±89.7	277.3±137.3	328.3±77.8	441.2±113.4	*P*<0.05
Number of branches per cell	449.5±144.7	717.5±392.3	741.4±239.3	380.3±73.7	*P*=0.147
Number of junctions per cell	206.6±66.2	370.4±203.8	375.1±131.3	348.7±69.8	*P*=0.114
Triple points per cell	190.3±60.9	319.6±180.3	347.7±120.8	321.9±63.6	*P*=0.120
Quadrupole points per cell	15.1±4.9	30.5±25.9	25.8±11.0	24.6±6.2	*P*=0.352

**P<0.01; ***P<0.001 (compared to mouse CTRT)